Landslides (2020) 17:985–1007
DOI 10.1007/s10346-019-01335-z
Received: 13 September 2019
Accepted: 5 December 2019
Published online: 6 January 2020

Honghui Wang · Donglin Nie · Xianguo Tuo · Yunshun Zhong

Research on crack monitoring at the trailing edge of landslides based on image processing

Abstract Currently, the frequency of landslides is increasing. Scientific monitoring methods are playing an essential role in effectively reducing landslide disasters. This paper proposes a method for identifying the cracks at the trailing edge of a landslide (TEL) based on image processing technology and adopts the custom interval median comparison algorithm (IMCA) to calculate the crack motion parameters. First, we perform a series of processes on the TEL images, including image preprocessing, Otsu's algorithm processing, and Canny edge detection processing, to identify the outline of the TEL. Then, we propose using the azimuth and displacement to characterize the motion of the cracks and using the IMCA to calculate the changes before and after motion of any two groups of cracks. Finally, we design a computer program using a free and open-source widget toolkit (named QT platform) based on the calculation model that corresponds to the proposed method, and we apply the crack monitoring test to a 3D simulation model, a gravel model, a soil model, and a collapsed body of the Panzhihua Airport landslide in southwestern China. From the results, it can be assessed that the method can identify the outline of the TEL and calculate the azimuth and displacement of two crack curves before and after motion. These two parameters can describe the movement of the trailing edge cracks of the monitored landslide. Thus, this method can be used in early warning system for landslide hazards.

Keywords Trailing edge of a landslide · Motion expression · Otsu's algorithm · Interval median comparison algorithm · Image processing technology

Introduction

From a global perspective, landslides remain one of the main natural disasters (Centre for Research on the Epidemiology of Disasters - CRED 2019). Large-volume landslides represent a persistent threat to human settlements and infrastructures in many mountainous areas worldwide; examples of such landslides include some of the landslides triggered by the May 2008 Wenchuan earthquake, such as the Daguangbao landslide (Yin et al. 2009; Huang and Fan 2013); the August 6, 2010, Mount Meager rock slide-debris flow in Canada (Guthrie et al. 2012); the March 22, 2014, Oso landslide in USA (Iverson et al. 2015); and the June 24, 2017, Xinmo landslide in China, which buried 64 houses, killed 10 people, and left 73 more people missing (Fan et al. 2017). Therefore, conducting landslide monitoring and early warning research is crucial for disaster prevention and mitigation.

When a landslide occurs, ground cracks (which often exist as a crack cluster that is also known as the crack zone) are formed between the sliding body and the stable body, which are generally curved due to the mechanical expansion (Zhou 2004). If the trailing edge has intermittent cracks and the crack length tends to be constant, the landslide has just begun to form. If thorough cracks occur at the trailing edge and the crack length increases, the landslide is in a state of continuous deformation. Therefore, monitoring the trend of the length of the trailing edge cracks of a landslide can reflect the displacement trajectory of the landslide body in a timely manner to provide early warnings for landslide disasters. Displacement monitoring techniques applied to landslides can be broadly subdivided in two main groups: geodetic and remote sensing (RS) techniques.

Geodetic surveying detects geometrical changes in landslide topography by measuring angles, distances (crack monitoring), or differences in elevation. Crack monitoring technology is widely used in the health assessment of infrastructures, such as roads, bridges, and tunnels. This technology is mainly used to monitor concrete cracking (Mohammad and Huang 2010; Gavilán et al. 2011; Wang et al. 2018; Qu et al. 2018) and to achieve the goal of disaster early warning. In landslide warnings, the traditional crack monitoring method involves installing tilt and displacement sensors on the landslide body to obtain the deformation data of the landslide in real time (De Dios et al. 2009; Yin et al. 2010; Wang et al. 2013; Ramesh 2014; Chen et al. 2015; Benoit et al. 2015), based on which the crack motion is evaluated. There are several disadvantages in this method: (1) high costs if we use high-precision sensors to obtain accurate deformation data, (2) presence of blind zones because the number of sensors in an arrangement is finite, and (3) low reuse rate of the sensors. Landslides will bury and damage sensors so that they may not be reused for long-term monitoring. Therefore, a more cost-effective way needs to be identified to achieve the target of monitoring the vast areas of landslides (e.g., the southwestern mountains area of China).

RS techniques are of interest as a possible operational tool to obtain spatially distributed information to deal with landslide monitoring, and there are three operation platforms: space-borne, air-borne, and ground-based platforms. RS techniques give the possibility to divide the unstable and stable areas in the landslide (Casson et al. 2005; Colesanti and Wasowski 2006; Wang 2009; Ghuffar et al. 2013; Pfeiffer et al. 2019). In recent years, the ground-based RS techniques are becoming more and more popular for landslide monitoring due to the flexible acquisition frequency and geometry, which can be adapted to any type of local environment (Delacourt et al. 2007). In addition, the ground-based platform can confirm whether there is real deformation of the landslide (Xu et al. 2019). They can be roughly subdivided in several main categories in landslide monitoring: ground-based synthetic aperture radar interferometry (GB-InSAR), terrestrial laser scanning (TLS), and terrestrial optical photogrammetry (TOP).

GB-InSAR is for the deformation monitoring of slopes (Noferini et al. 2006), tectonic (Massonnet et al. 1993), and volcanoes (Wadge 2003), etc. In 2003 (Tarchi et al. 2003), a landslide was monitored by GB-InSAR for the first time. It can reach high data accuracy possible (millimetric accuracy) and work during the night and any type of weather conditions while require a large

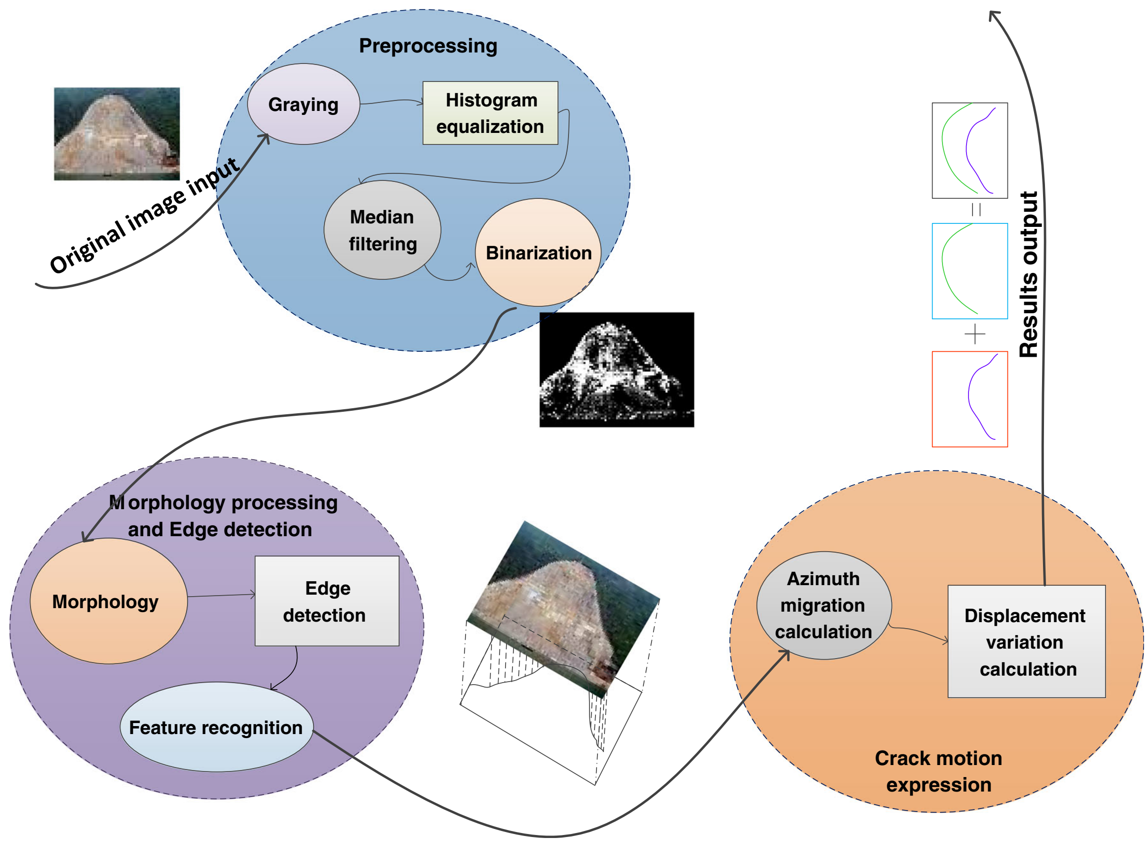

Fig. 1 Research plan and methods

initial investment and skilled crew for operation. Readers can find the principle in (Pieraccini et al. 2001; Tarchi et al. 2003) and the current applications in (Ferrigno et al. 2017; Frodella et al. 2018; Pieraccini and Miccinesi 2019).

TLS can produce good results for landslide deformation monitoring (Prokop and Panholzer 2009), thanks to its capability to derive from the acquired point cloud an accurate and regularly structured digital elevation model (DEM) of land surfaces (Briese

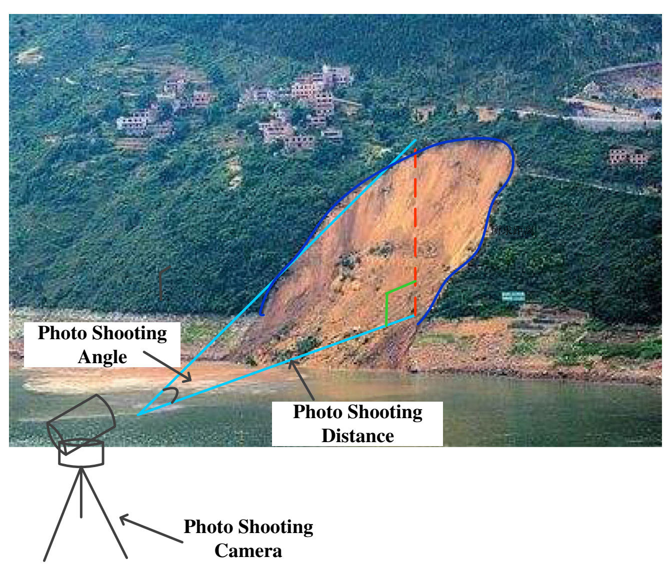

Fig. 2 Schematic diagram of image acquisition

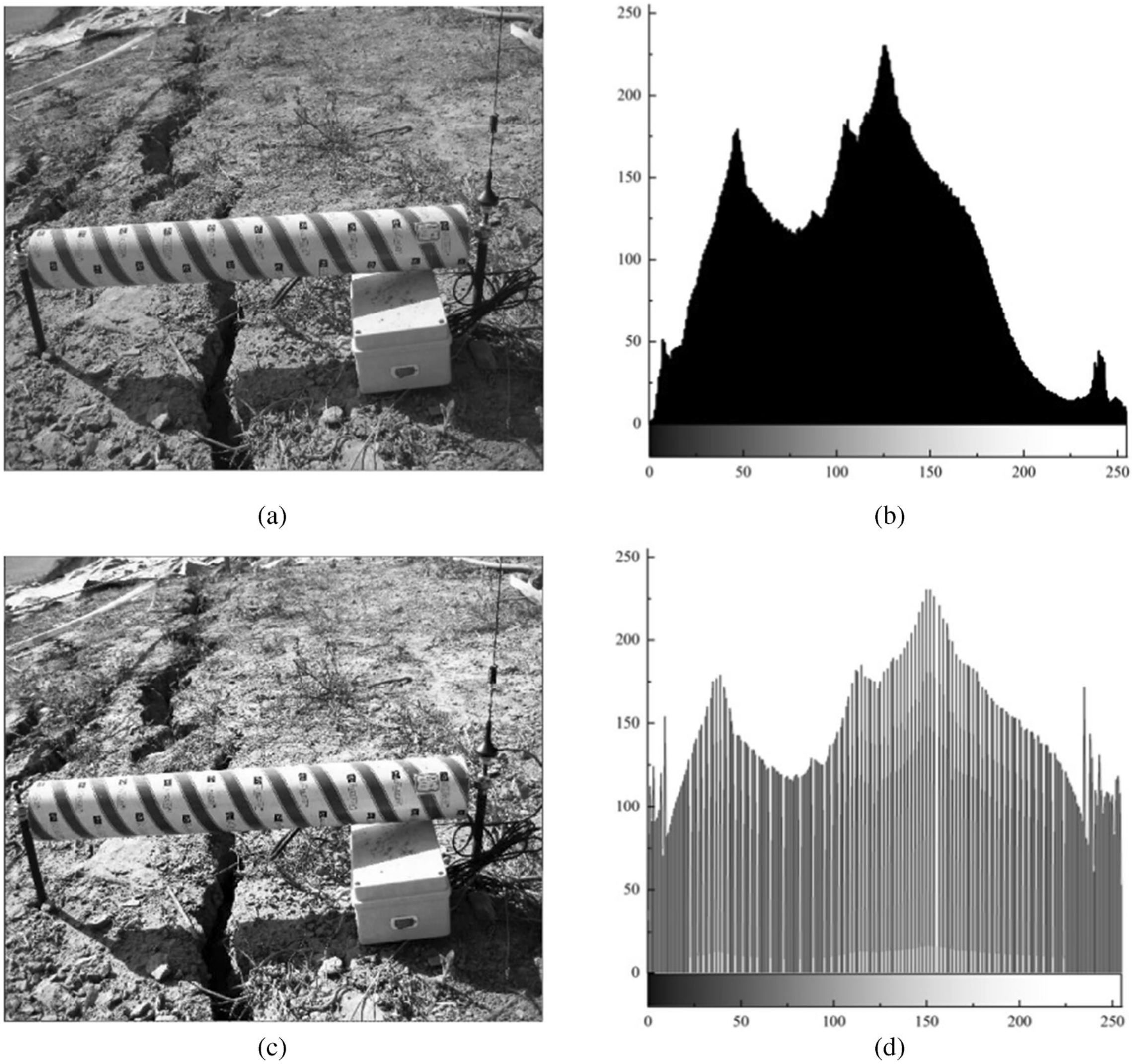

Fig. 3 A sample image of a landslide crack monitor and its histogram, before and after image histogram equalization. Image size = 256 by 256. *X*-axis: 0 = black, 255 = white. *Y*-axis: the number of pixels (was compressed to 0–255)

2010). The technology can be high data accuracy and provide an easily understandable image, while it needs skilled crew for operation and a large amount of computational resources for spatial data visualization (Travelletti et al. 2012).

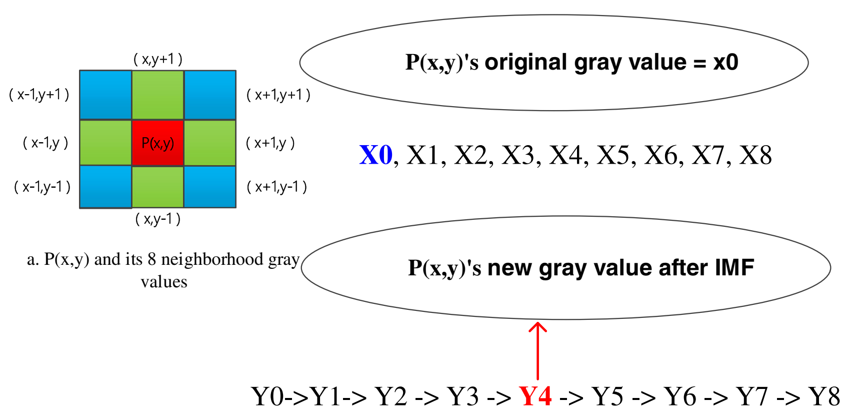

Fig. 4. Schematic diagram of the IMF

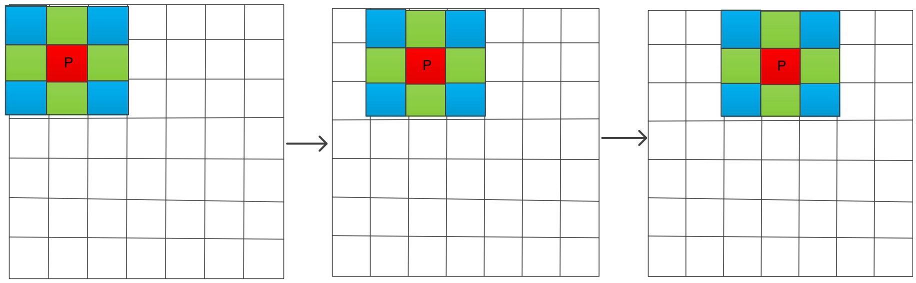

Fig. 5 Schematic diagram of structural element traversal

TOP consists in acquiring digital RGB images represented using a matrix of intensity values recorded at each pixel of the charge-coupled device (CCD) of the camera from a spot very close to the ground (Jiang et al. 2008). It costs much lower than GB-InSAR and TLS. And it can compute 2D displacement fields. The major drawbacks of TOP are (1) weather and illumination changes affect the images quality and (2) the ground control points (GCP) are necessary for camera calibration. In recent years, some techniques, such as machine learning, computer vision, and pattern recognition, are combined with TOP. These new techniques have a great potential to provide topographic information for geoscience applications at significantly lower costs than classical topographic and laser scanning surveys (Stumpf et al. 2015).

Terrestrial surveys by total stations and GNSS receivers are other most widely used and well-known techniques for monitoring landslides. They are useful when we have to measure the positions of single points which are materialized on the terrain. The accuracies achieved using these surveying methods are very high, but the points that can measure are few and they must be accessible (Barbarella and Fiani 2013).

A digital image processing method was proposed in the 1950s. This method uses image data collected by cameras and other image acquisition devices as a data source to extract the target area information using operations such as image denoising, image enhancement, and image segmentation. This method has been widely used in road crack detection and bridge crack and deformation monitoring (Peng et al. 2015; Cho et al. 2016). This method can replace the fixed-point sensors, and it has a wider monitoring area with a more remarkable effect. Therefore, researchers have tried to combine this method with GIS and satellite remote sensing images for landslide monitoring. For example, Rawat et al. (2017) introduced a method for developing landslide models using multi-criteria decision analysis in GIS and remote sensing techniques. In this method, the landslide merged data from 2011 to 2012 were visually interpreted by satellite images to establish digital elevation maps (DEMs) with different grades to monitor landslide deformation. Riedel et al. (2010) combined image processing technology with spatial analysis technology by segmenting an original landslide image into partial images and eliminating interference factors, such as drainage channels, highways, and old slips, to obtain new slips on the image. Stumpf et al. (2013) used high-precision subdecimeter spatial resolution aerial image as the carrier and divided the landslide motion into three basic modes: stretching, sliding, and tearing. This method adopted edge detection algorithms, such as the Canny and Sobel operators, as the processing chain to distinguish target cracks and vegetation. Rothmund et al. (2017) processed multi-temporal high-resolution aerial images to obtain multi-temporal 3D point clouds and multi-time orthogonal mosaic renderings in order to map slowly moving alpine landslides.

Based on these previous studies, some researchers have also proposed improved algorithms to promote monitoring. James et al. (2017) proposed a structure-from-motion algorithm (SFM), which effectively detects and eliminates stepped artifacts close to 50 mm by automatically and semi-automatically identifying ground control points (GCPs) in images to effectively monitor the speed changes of landslides. Gance et al. (2014) proposed a target detection and tracking (TDT) algorithm for the fast detection of a target's continuous displacement at subpixel precision in landslide images. Yang and Chen (2010) proposed a method to detect the distribution of landslide changes by detecting vegetation change after landslide event. This method subtracted images before and after a landslide event to obtain the pixel variation range of the landslide activity. The modal filter is used to suppress the boundary error to determine the final landslide distribution map.

In summary, for landslide, the abovementioned methods pay more attention to landslide identification, deformation, and motion monitoring. In general, the scale of the research is large. The objective of this work is to focus on how to monitor the trailing edge of a landslide (TEL) based on image processing techniques.

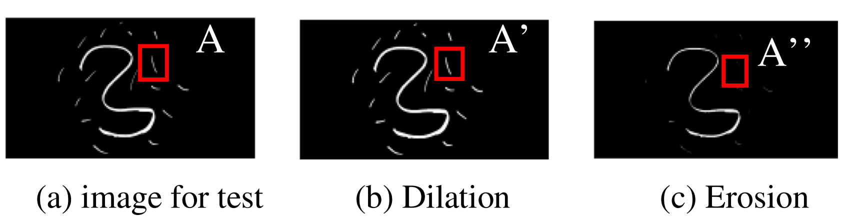

Fig. 6 Schematic diagram of IMP

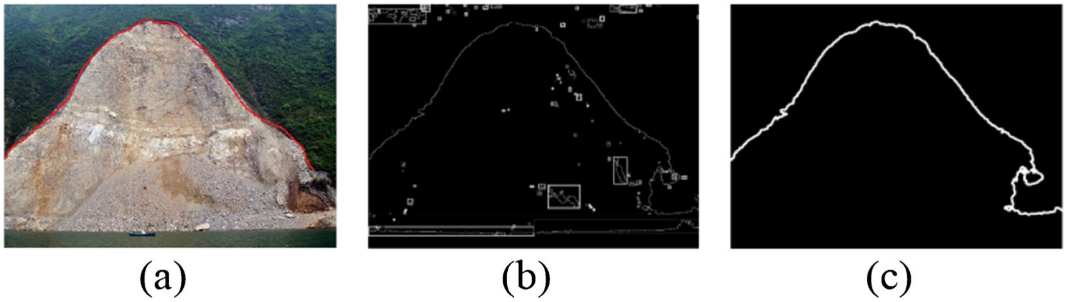

Fig. 7 **a** A sample image of a landslide. **b** The image after Canny edge detection and feature recognition. **c** The image after target curve shaping

First, we propose a set of data methods for processing the TEL images. Then, through four sets of case studies, we verify the above method and give the limitations. In addition, the paper also studies the expression of the motions of the trailing edge cracks of the same landslide body at different stages.

The research plan for this paper is shown in Fig. 1.

First, a high-precision camera is erected in front of the landslide scene to directly obtain landslide images for each stage of the landslide event, as shown in Fig. 2. Then, the preprocessing, morphological processing, and edge detection techniques in the image processing method are used to accurately and effectively identify the sequential curves of the TEL at various stages. Finally, the changes in the displacement and azimuth angles that are generated by the curves between adjacent stages are calculated by the interval median comparison algorithm (IMCA, the details will be given in the "Motion displacement" section) and aggregated into a model to reflect the overall landslide movement.

Here, we further discuss about the image preprocessing. Our goal is to detect the crown of the TEL. In computer vision and image processing, the image morphology processing and edge detection methods can achieve that goal. Actually, morphology, which is also known as image algebra, is a mathematical tool for analyzing binary images. The basic idea is to use a structural element with a certain shape to measure and extract the corresponding shape in the image for image analysis and recognition. Therefore, we need to identify one method to convert the input color images into binary images. Our image preprocessing is specially designed for this conversion, and it includes four steps: the image graying (IG), image histogram equalization (IHE), image median filtering (IMF), and image binarization (IB). The goal of IG is to convert the color images to black and white images (one kind of grayscale image), which reduces the amount of data for computing. The IHE function enhances the contrast of the image to make the details of the gray areas in the image clearer. IMF is a nonlinear smoothing technique to eliminate the images' noise. IB converts the grayscale images to binary images, which can then be processed in the next step: morphology processing and edge detection.

The rest of the paper is organized as follows. First, the "Methodology" section introduces the proposed research methods in details, including the image processing steps, corresponding algorithms, crack motion expression, and QT-based test software based on the above processing steps. Then, the "Case study" section introduces the case study and uses four scenarios to validate the approach that is described in the "Methodology" section. Finally, the conclusions are presented in the "Conclusions" section.

Methodology

Image preprocessing of landslide cracks

It is well known that from the point of view of color, the trailing edge portion of a landslide exposes the color of the rock and soil. In contrast, the relatively stable inactive parts usually have color difference. For example, the trailing edge of a landslide in southwestern China is usually covered by vegetation. This feature provides a theoretical basis for the identification of the crack curve of the back edge of a landslide based on image processing.

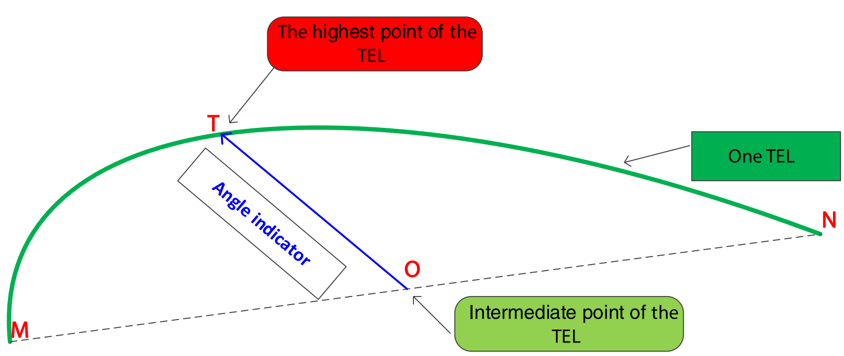

Fig. 8 Schematic diagram of one TEL's angle indicator line

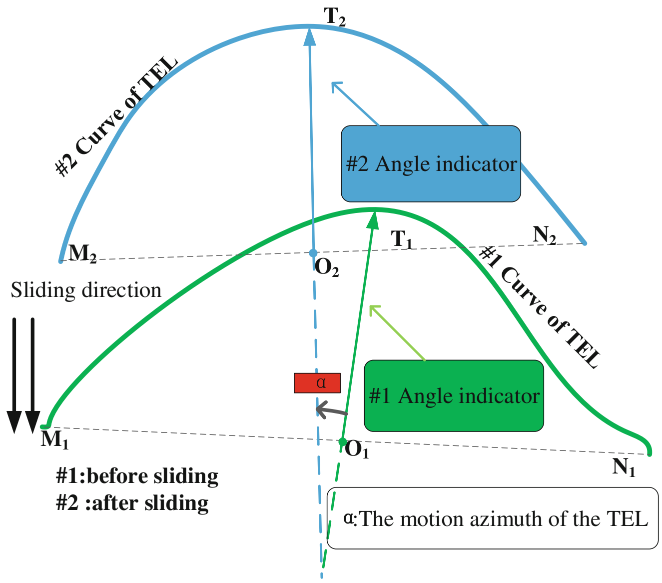

Fig. 9 Schematic diagram of the motion azimuth of the TEL

Image graying

Since CCD images are color images, the amount of calculations required for processing these images is large, which results in a slower computer processing speed. Therefore, we usually convert CCD color images into corresponding grayscale images for processing (Cheng et al. 2001). We name this process IG. The most often used image graying method is the weighted averaging method, which performs a weighted averaging of the three-channel component of the color image to obtain a grayscale image. The expression formula of the grayscale image is as follows (considering the physiological structure of the human eye) (Saravanan 2010):

$$f = 0.299R + 0.587G + 0.114B \tag{1}$$

where R, G, and B are the values of the red, green, and blue color channels of the pixel, respectively.

Image histogram equalization

It is well known that an image with a uniform distribution of gray values generally has a high contrast ratio. Image histogram equalization is a method that transforms a grayscale image into a new image with a uniform distribution of gray histograms. The basic idea is to broaden the gray level of the image with more pixels and to compress the gray level of the image with fewer pixels (Sim et al. 2007), thereby expanding the dynamic range of the original value, improving the contrast, and making the image clearer. The image gray level broadening effect is shown in Fig. 3.

Figure 3 a and b show a landslide crack monitor's image with its equivalent histogram. The output image of the input image after IHE is given in Fig. 3 c and d. The grayscale of Fig. 3b is concentrated. After IHE processing, a graph d with a more uniform gray distribution is obtained, which corresponds to a higher contrast. This result demonstrates the performance of the IHE method at enhancing the contrast of an image through dynamic range expansion.

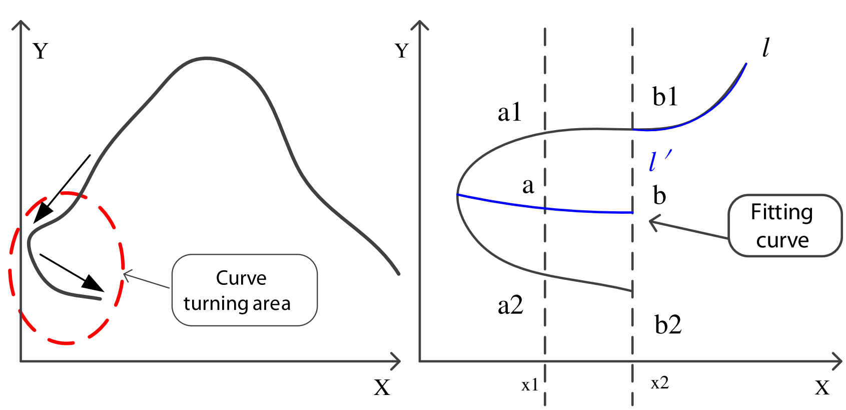

Fig. 10 Schematic diagram of the IMCA

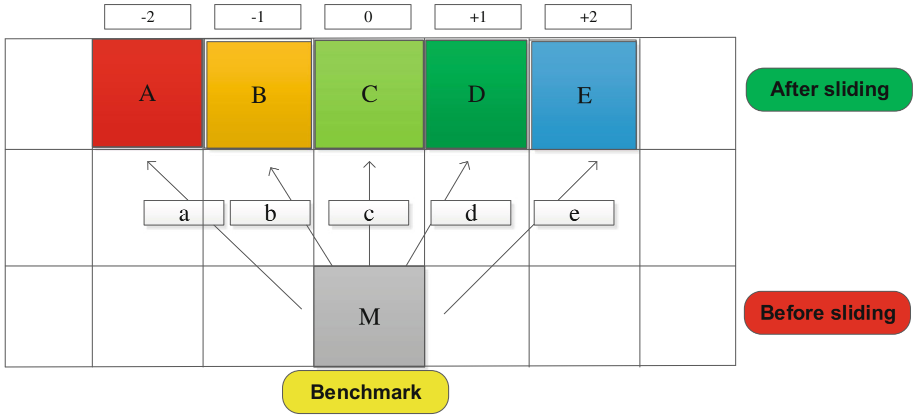

Fig. 11 Schematic diagram of TECL's pixel point displacement

Image median filtering

IMF is a nonlinear smoothing technique (Sun and Neuvo 1994; Tao et al. 1999), which essentially uses the median value of the grayscale rank value of the neighborhood pixel of the target pixel as the new grayscale value of the target pixel, in order to eliminate the image noise. The example of a 3×3 neighborhood matrix is shown in Fig. 4a. This kernel is also called the structural element. First, we sort the 8 neighborhood gray values x1–x8 and xo of the target pixel point P (x, y) (the gray value is xo) from small to large, as shown in Fig. 4. The median value Y4 of the new sequence is then taken as the new gray value of the target pixel point P (x, y) after IMF.

Next, we follow the same principle. The structural element is traversed through the original image (as shown in Fig. 5), and the new gray value of all target pixels is obtained. In this way, the image noise can be smoothed.

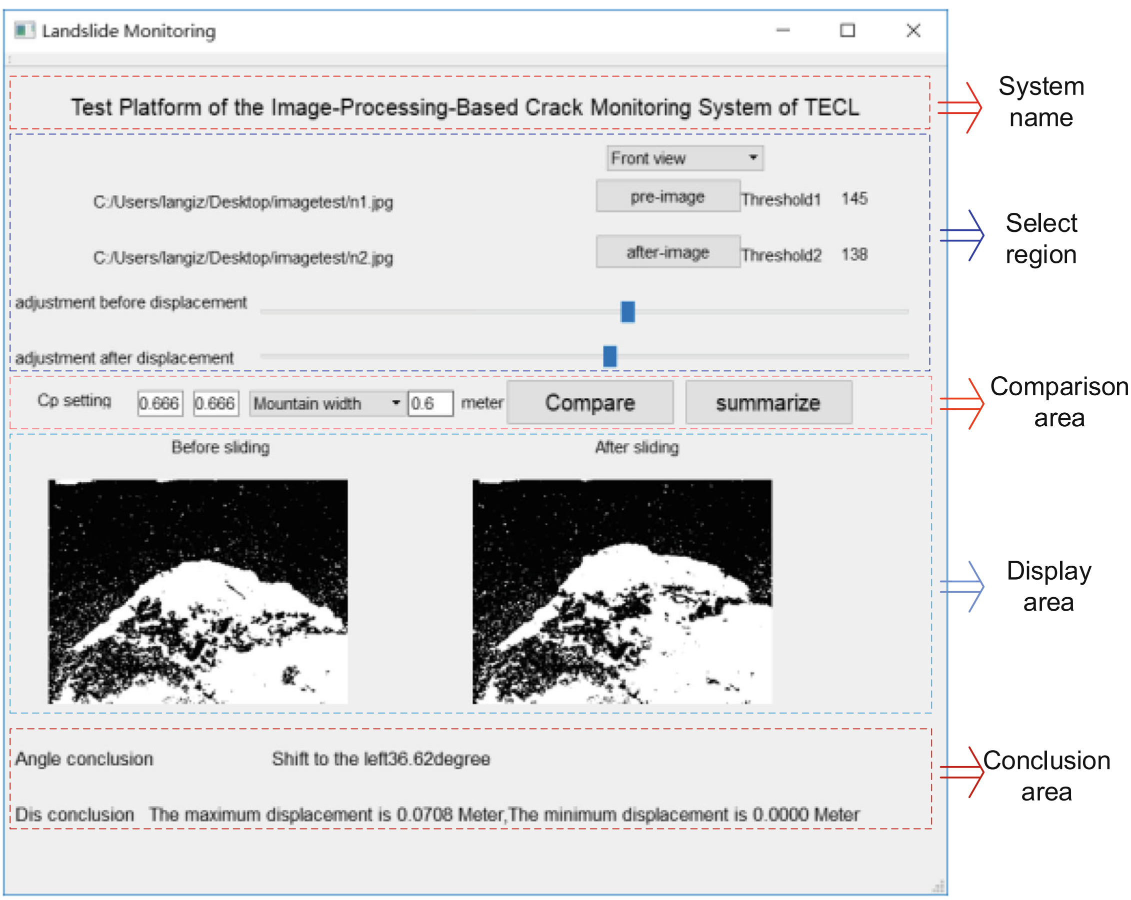

Fig. 12 Screenshot of the test software interface

Fig. 13 Original landslide picture

It should be noted that the larger the structural element is, the better the processing effect on noisier points is. However, if the structure element is too large, it is easy to cause image distortion and lose information. Therefore, the size of the structural element should be set according to the actual situation. Common structural element sizes are 3 × 3, 9 × 9, and so on.

Image binarization

IB is an image segmentation method, which is used to enhance the characteristics of the target image (Gatos et al. 2006). We compare the gray value of the pixel with the threshold value. If the gray value is less than the threshold value, the gray value is set to 0. Otherwise, the gray value is set to 255, which makes the image appear in only black or white. The appropriate selection of the threshold plays an essential role in image binarization. One popular thresholding method is the Otsu algorithm (Otsu 1979; Sezgin and Sankur 2004). The basic steps are as follows. (1) We use a threshold T to separate the image into two parts: foreground and background. (2) Then, we calculate the interclass variance between the foreground and background regions. (3) When the interclass variance is the largest, the difference between these two parts is also the largest, where the T is the optimal threshold. This method can minimize the probability of misclassification between the foreground and background regions. In addition, Otsu provides an adaptive threshold, which can automatically calculate a recommended threshold based on the characteristics of the input image. This function is beneficial for landslide image processing.

It should be noted that, for general CCD images that are captured by cameras, because of the objective factors such as focusing and light, the threshold that is calculated by the Otsu algorithm is not necessarily the best. We can dynamically adjust the threshold size to obtain the best binarization effect. In other words, we (users) can fine-tune the left and right to better segment the foreground area (e.g., rock and soil) and background area (e.g., vegetation).

Image morphology processing and edge detection

Image morphology processing

The most basic operations in morphology include dilation and erosion which process the white area of the image (the highlighted part) and not the black area. Dilation expands the highlighted part of the image. Dilation combines all background points that are in contact with the foreground area into the object and can be used to fill the holes in the foreground area. Erosion is a process of shrinking the boundary inward and can be used to eliminate small and meaningless foreground areas.

To show the effects of dilation and erosion, we used a black marker to draw a picture on white paper and then preprocessed it using the IG, IHE, IMF, and IB methods. Considering that the object of the dilation and erosion processing is white, we exchanged each pixel value, e.g., 0 to 255, and 255 to 0, to form Fig. 6a.

Figure 6 shows a diagram of the effect of the closure operation (dilation followed by erosion) on the binary image of the hand-drawn test image that includes some noise (not just salt and pepper noise). It can be seen from the figure that the small foreground outline in region A' is obviously larger than that in A foreground outline. Because of the erosion effect, the small foreground outline has basically disappeared in region A".

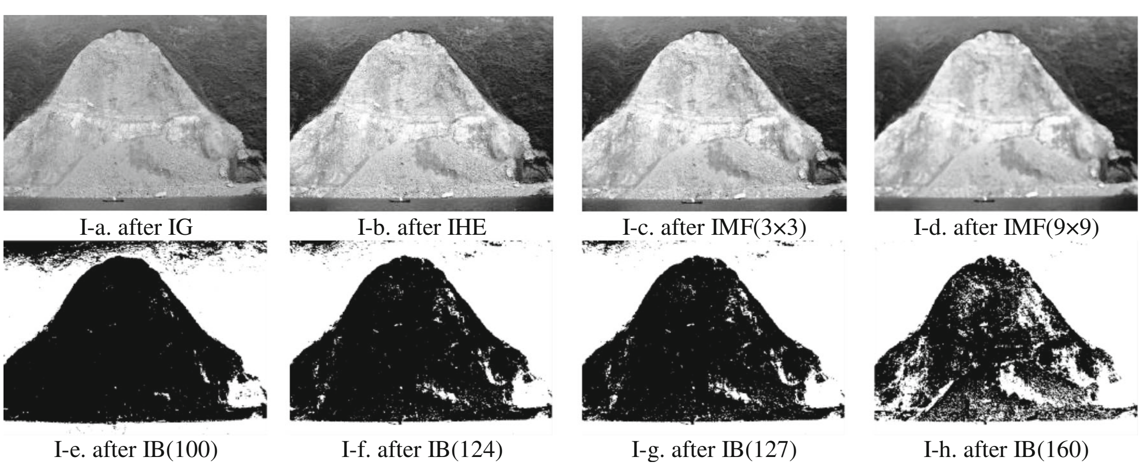

Fig. 14 Processed images (I)

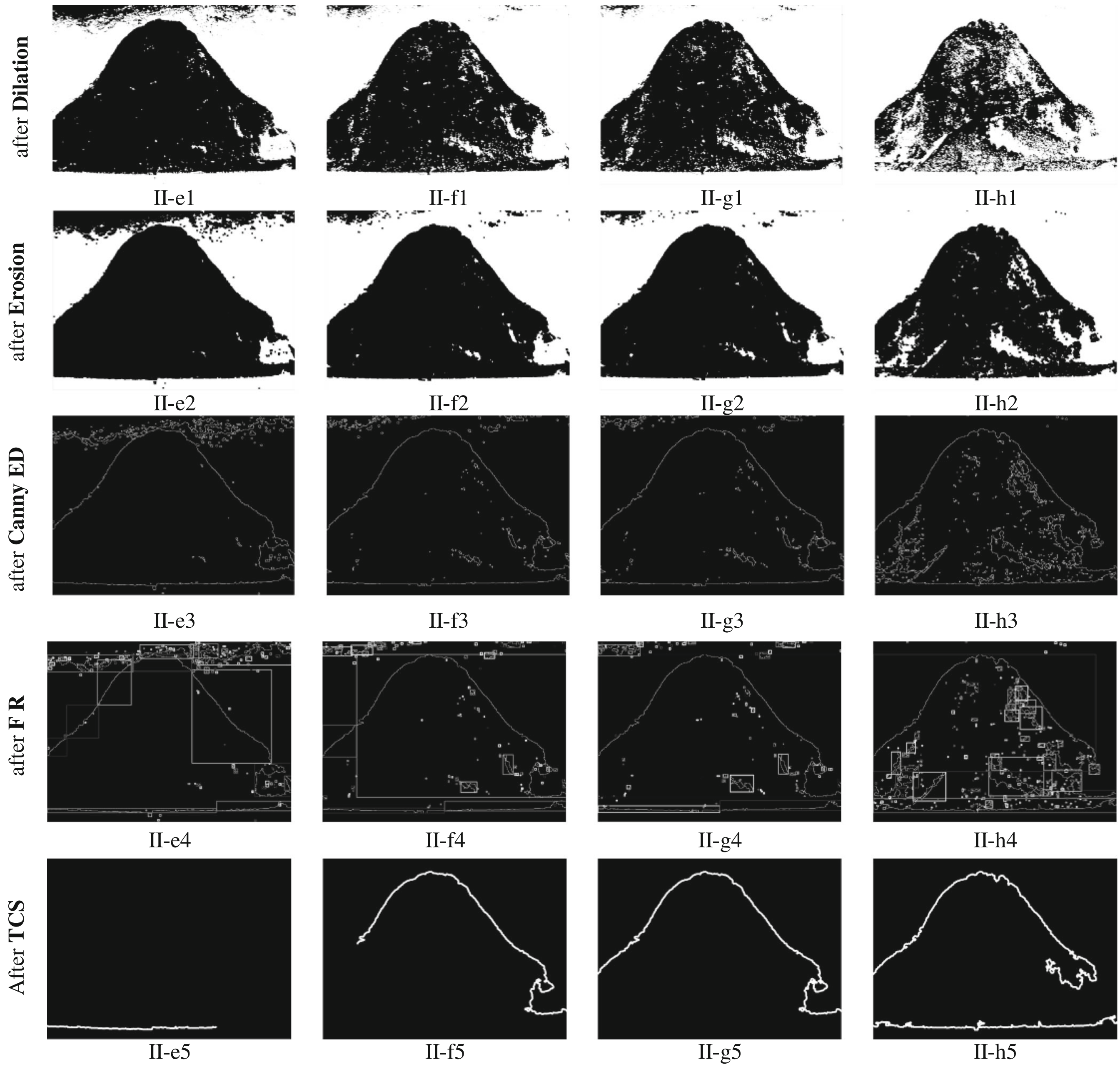

Fig. 15 Processed images (II)

Therefore, the closure operation is often used to connect near foreground areas and to eliminate the small voids without changing. To better describe the trend of the crack curve on the TEL, this paper adopts the closure operation method to conduct the process.

Edge detection

Edge detection (Marr and Hildreth 1980) uses the discrete gradient approximation function to find the gray jump positions of an image's gray matrix according to the gradient vectors of the two-dimensional gray matrix, and then connects the points of these positions to constitute the edge. Nevertheless, we can hardly see the ideal gray jump. In addition, most sensors have low-frequency filtering characteristics, which will make the step edge become a sloped edge, and it seems that the intensity change is not instantaneous, but rather it spans a certain distance. Therefore, filtering is performed first in edge detection. Compared with mean filtering and median filtering, Gaussian filtering can preserve the overall gray distribution characteristics of the image and improve the edge detection accuracy. In addition, landslide CCD images may be acquired at low illumination levels, and this acquisition environment is more likely to introduce Gaussian noise. Therefore, here, we adopt the Gaussian filter. The Canny operator (Canny 1986) is the most commonly used edge detection algorithm that also uses Gaussian smoothing. The steps are as follows:

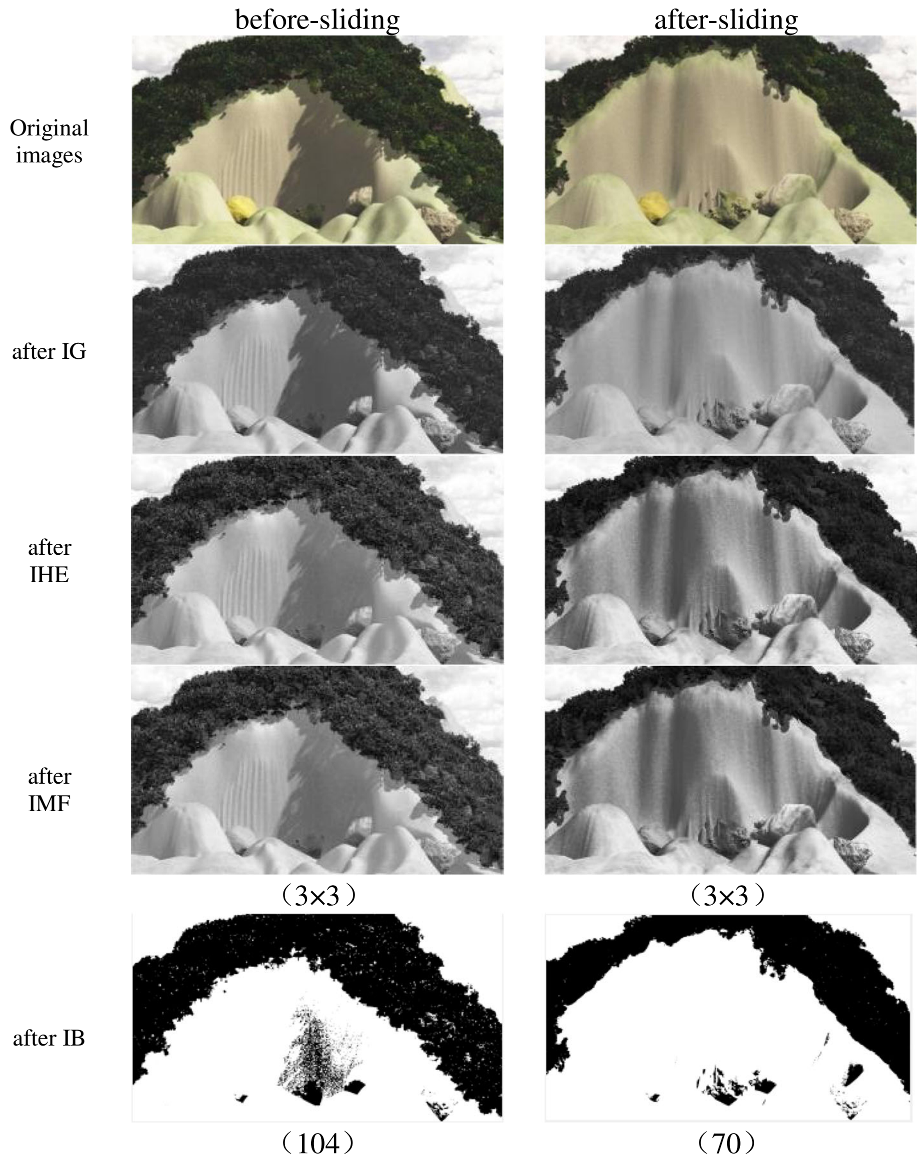

Fig. 16 Processed images of the 3D model

Step 1: Gauss denoising

To reduce the noise interference, Gaussian denoising processing is required for the image. The smooth image is obtained by the convolution of the Gauss function and the image. The two-dimensional Gauss function formula is as follows:

$$G_i(x,y) = \frac{1}{2\pi\sigma^2} e^{\frac{-(x^2+y^2)}{2\sigma^2}} \tag{2}$$

Step 2: amplitude and direction

According to the Canny algorithm, when processing grayscale images, we can use the first-order finite difference to calculate the gradient values (i.e., the rate of change of grayscale values). That is, we calculate the differences between adjacent pixels in the x and y directions instead of calculating the first derivatives in the x and y directions. Therefore, the gradient amplitudes along the x and y directions are as follows:

$$\begin{aligned} P[x,y] &= \frac{f[x+1,y]-f[x,y]+f[x+1,y+1]-f[x,y+1]}{2} \\ Q[x,y] &= \frac{f[x,y]-f[x,y+1]+f[x+1,y]-f[x+1,y+1]}{2} \end{aligned} \tag{3}$$

where $f[x,y]$ is the gray value of the pixel (x, y). Thus, the amplitude and direction of the point are as follows:

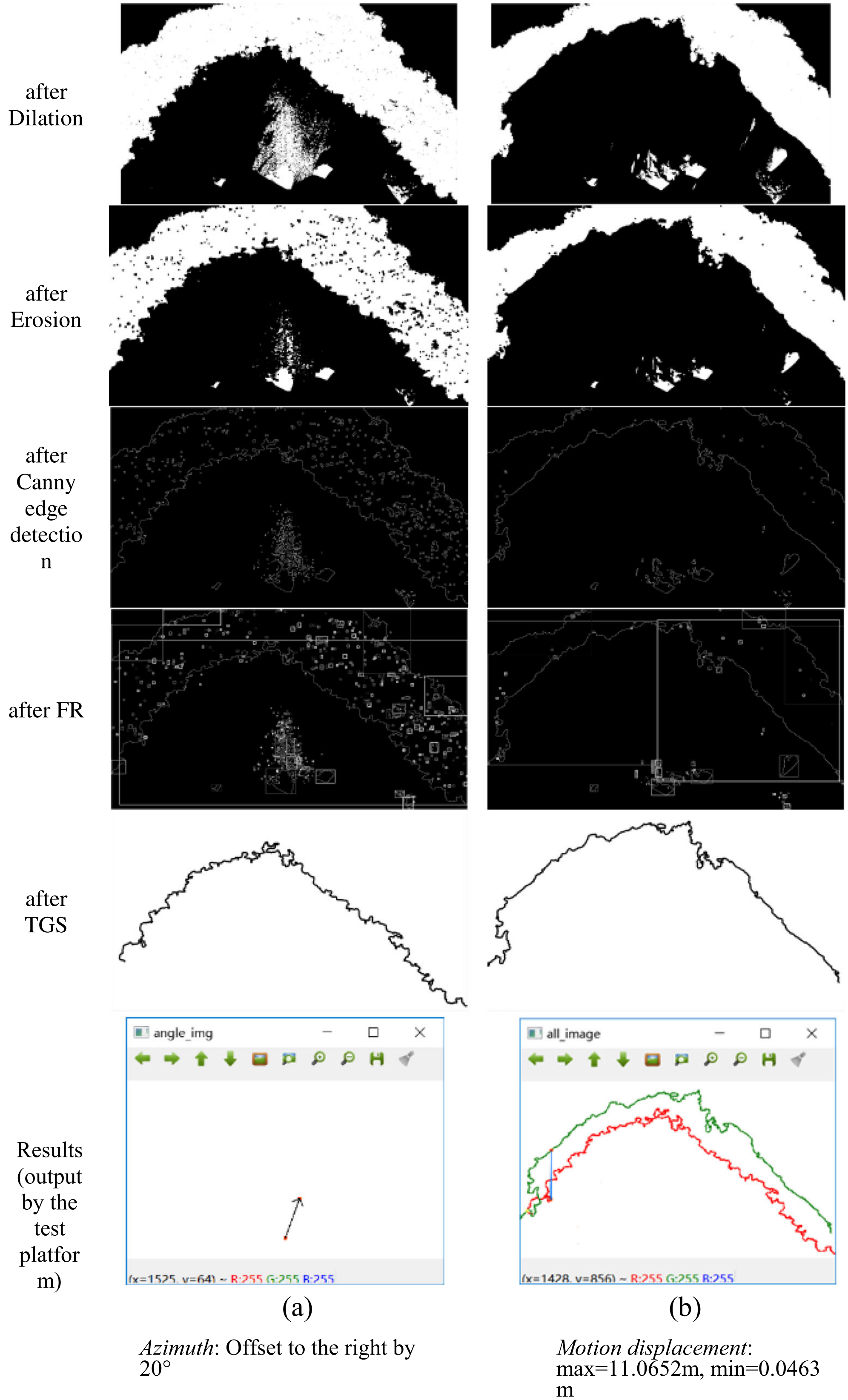

Fig. 16 continued.

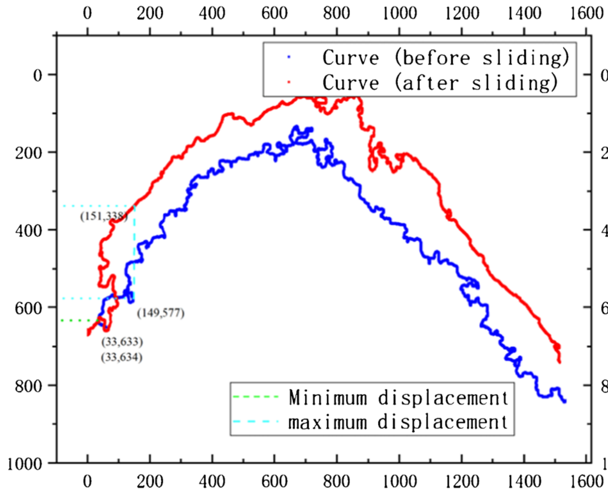

Fig. 17 Curve based on calculated data (3D model)

$$M(x,y) = \sqrt{P[x,y]^2 + Q[x,y]^2}$$
$$\alpha[x,y] = \arctan\left[\frac{Q[x,y]}{P[x,y]}\right] \tag{4}$$

Step 3: nonmaximum suppression

The global gradient is not enough to determine the edge. It also needs to suppress the nonmaximum value and retain the local gradient maximum point, which can make the image edge thinner and remove most of the false edges.

Step 4: double threshold detection

The method for reducing the number of false edges in the Canny algorithm uses double thresholds: t_1 and t_2 ($t_1 < t_2$). If the amplitude of pixel T is lower than t_1, T is retained as an edge pixel. If the amplitude of pixel T is higher than t_2, T is discarded. If the amplitude is between t_1 and t_2 and the connection of the pixels is larger than t_1, T is retained as an edge pixel; otherwise, it is discarded. Here, we use the Otsu threshold as the high threshold t_2 and half of the Otsu threshold as the low threshold t_1.

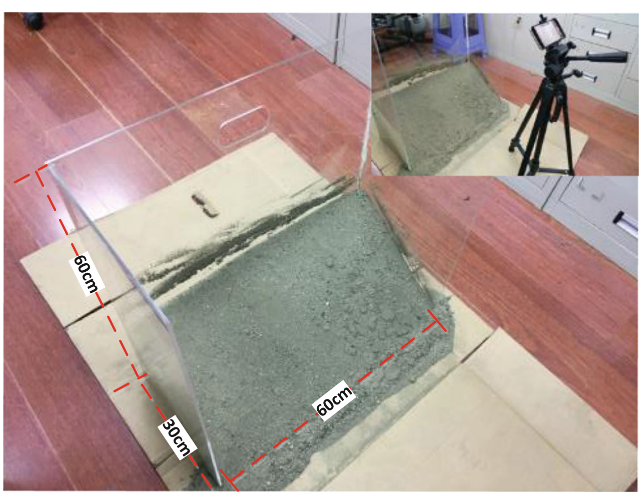

Fig. 18 The gravel landslide model

Feature recognition

An image that is processed by Canny edge detection contains many image regions that are composed of neighboring foreground pixels, which are defined as connected regions. To better describe this procedure, we use one landslide photo as the input image and the processed images are also given in Fig. 7.

As seen from Fig. 7b, there are two types of connected regions: a connected region R_e, including a trailing edge crack curve (white curved line), and a connected region R_n, including an interference curve (white small circle). The task of this step is to eliminate the interference connected region R_n and extract the connected region R_e including the trailing edge.

We assume that the height of image b is H pixels, and the width is W pixels. We project each R_i in graph b into the H and W directions of the image to obtain $H_i^{'}$ and $W_i^{'}$, respectively, and then calculate the following: $P_i^H = H_i^{'}/H$ and $P_i^W = W_i^{'}/W$. Here, we want to artificially set two references P^H and P^W. For any R_i, if $P_i^H \geq P^H$ and $P_i^W \geq P^W$, the foreground area package contains the crack curve. Otherwise, it is not considered to be the foreground connected area where the cracks are located.

From the actual characteristics of a landslide image, we know that R_n is much larger than R_e. Therefore, we usually set P^H and P^W to be greater than or equal to 1/2. We have designed the software interface to set these two parameters (please see the Cp setting in Fig. 12).

Target curve shaping

The number of white edge points and the coordinates of the pixel points are obtained by progressively scanning the crack curve of the trailing edge of a landslide from top to bottom. The set of coordinates are called the set of pixels of the crack curve of the trailing edge of the landslide (see Fig. 7c).

Crack motion expression

The cracks that we study here are those that are distributed at the trailing edge of the landslide and that are perpendicular to the main sliding direction, which are formed by the material sliding down along the sloping rock under the effect of gravity. Monitoring the crack trajectory can better predict the direction of the slide. To better describe the crack motion, we have defined two parameters: the azimuth and motion displacement.

Azimuth definition

Exploring the azimuthal variation of the outline of the TEL can predict the possible sliding direction of the cracks at the trailing edge of a landslide. To the best of our knowledge, the scientific literature lacks a method to define the trailing edge of a landslide. Therefore, this paper customizes an algorithm to define its azimuth.

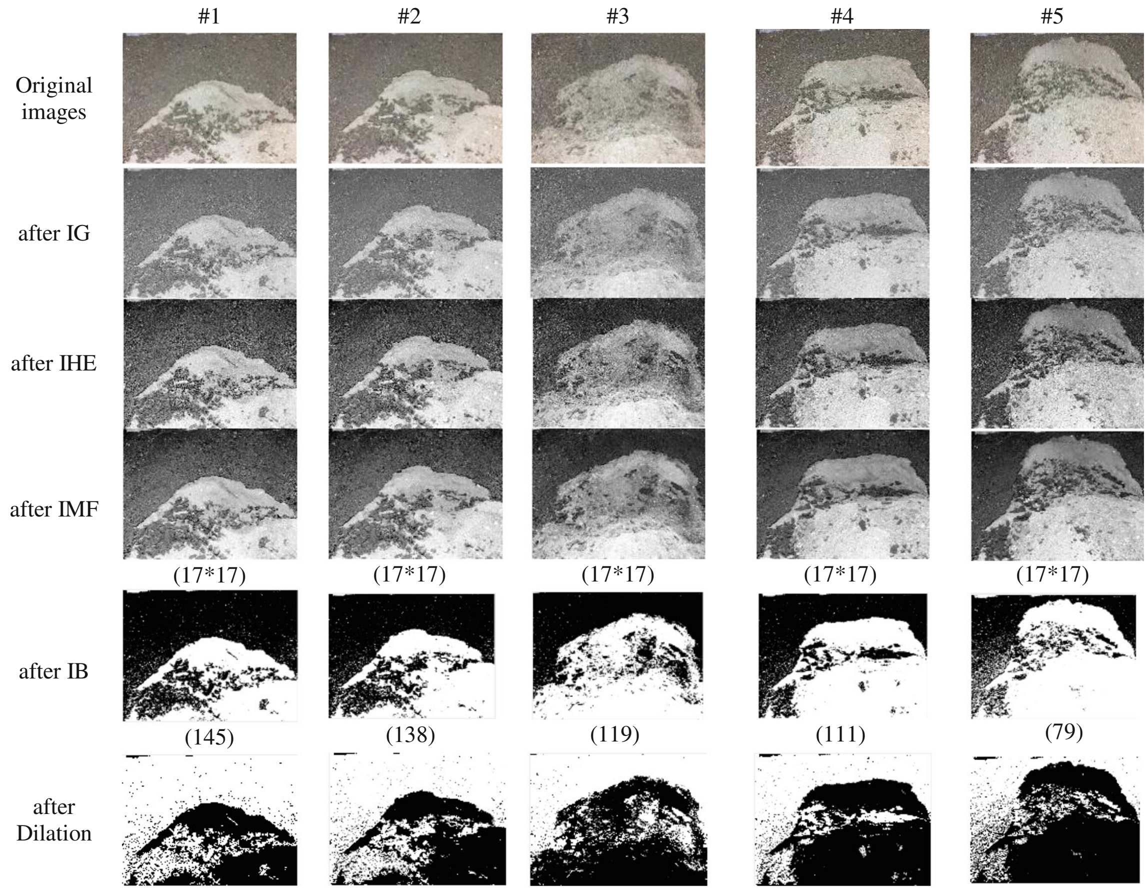

Fig. 19 Processed images of the gravel model

As shown in Fig. 8, we note that the highest point of the TEL is T, the two endpoints are M and N, the midpoint of MN is O, and the connection OT is used as the angle indication line of the TEL.

As shown in Fig. 9, we assume that the landslide has a new slide along the main sliding direction, causing the crown of the trailing edge to change from #1 to #2. Referring to the practice in Fig. 8, we extend the two angle indicator lines, and the angle α between the two lined represents the azimuth of this slide.

Motion displacement

During landslide development, the cracks at the trailing edge of the landslide tend to undergo unpredictable deformation along with the movement of the sliding body, including but not limited to, front and rear movement, left and right movement, crack coverage (or even disappearance), new cracks development, etc. How to determine the correspondence between the pixel points of the crack curve before and after the motion becomes the key point of the postimage processing.

We know that there may be curve turning (as shown in Fig. 10) in the identification of the trailing edge crack curve of the landslide. As shown in the red dashed box in Fig. 10, at the beginning, the curve extends in the negative direction of the X-axis. After passing point A, the curve begins to extend in the positive direction of the X-axis. Therefore, in this curve turning area, the curve has the characteristics of a multivalued function. For example, the functional values of x1 are a1 and a2. The problem is which value should be used to calculate the motion displacement. Therefore, this paper proposed the custom IMCA to eliminate curve turning. The specific steps of the IMCA are as follows.

First, we need to convert the trailing edge crack curve into a monotonous curve. When a turn occurs on the crack curve, we take the average value of all the y values corresponding to x as the new y value. Take Fig. 10 for example. The y values to which x1 corresponds are a1 and a2, and the y values to which x2 corresponds are b1 and b2. Therefore, we use the average of a1 and a2 and the average of b1 and b2 as the new y values a and b, respectively. In this way, the whole turning zone in a curve can be traversed with respect to x to form a new fitting curve l' (blue line).

Then, we calculate the distance value before and after the displacement of each pixel on the curve. Since the correspondence between each pixel point cannot be strictly tracked before and after the landslide motion, the displacement interval is used to determine the possible displacement change of the pixel. As shown in Fig. 11, we assume a pixel point M. After one sliding, the possible positions of the pixel are A, B, C, D, and E, and each point is separated by 1-pixel unit.

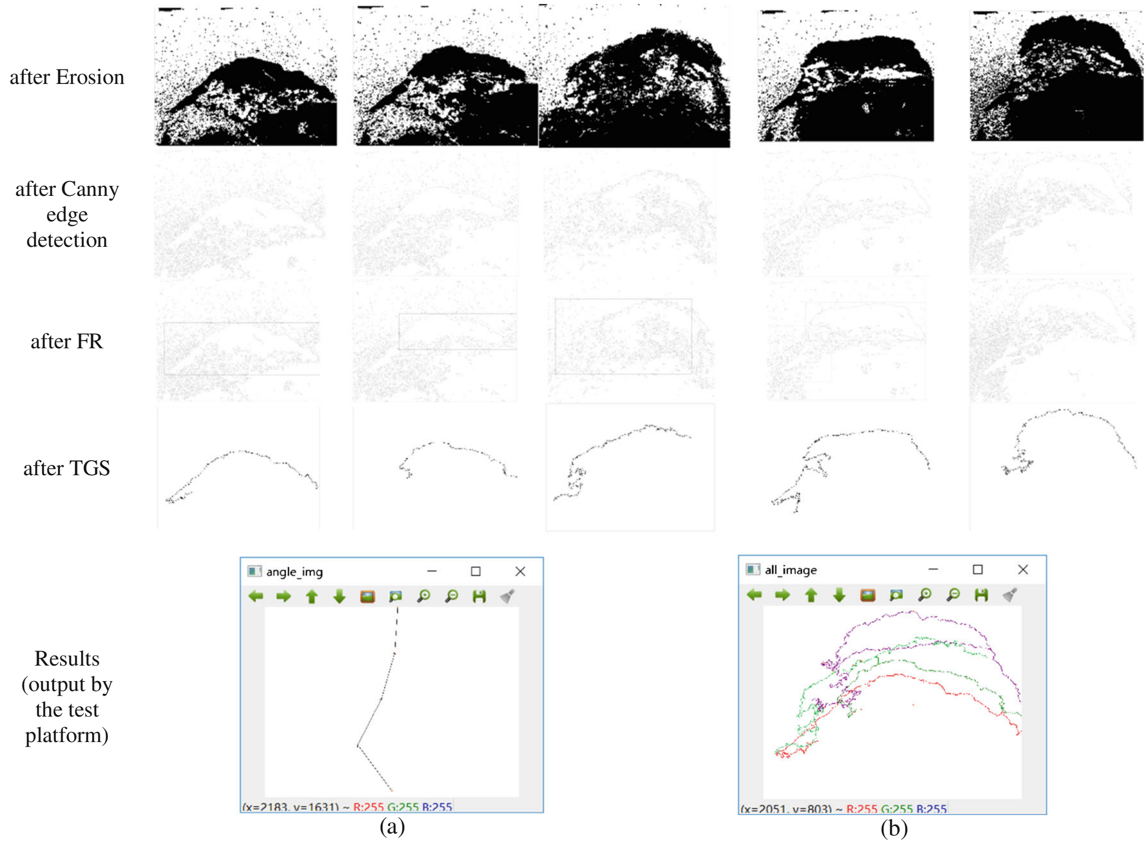

Fig. 19 continued.

Finally, the distances a, b, c, d, and e between the reference pixel point (M) and the five possible displacement points (A, B, C, D, and E) are individually calculated. The minimum value min{a, b, c, d, e} and the maximum value max{a, b, c, d, e} are selected as the displacement change interval of the reference point.

Conversion of image scale and physical scale

The algorithms that are mentioned in this paper all use pictures as the processing source, and the displacement results that are calculated by computer programs are all in pixels. Therefore, the image scale data needs to be converted into physical scale data.

The scale conversion relationship actually indicates how many physical distances are represented by one pixel (Li 2006). Here, scale theory is used for the relational transformation. If the scale conversion parameter is k, x1 and y1 are the image scale lengths and x2 and y2 are the physical scale lengths.

$$K = \begin{cases} \frac{x1}{x2} & x \text{ direction} \\ \frac{y1}{y2} & y \text{ direction} \end{cases} \tag{5}$$

First, we record some of the conventional parameters of the landslide, including the mountain height, mountain width, and so on. Then, we calculate the ratio of these parameters to the area pixel size in the corresponding picture to obtain the conversion scale factor k. Finally, the actual displacement of the cracks can be obtained by multiplying k by the pixel displacement of the trailing edge crack curve of the landslide.

Test platform based on QT

To better use the method that is proposed in this paper to perform TECL displacement monitoring, we developed QT-based test software (the software interface is shown in Fig. 12). The proposed image processing algorithm is based on the OpenCV library and is loaded to the QT software platform. The user only needs to input the landslide image source to obtain the curve recognition result. The user can also manually change the image binarization threshold to obtain the best curve recognition result.

The steps to operate the software are:

Step 1: Open the software, determine whether it is a front view or a top view according to the input image, and click the corresponding option.

Step 2: Click the “pre-image” and “after-image” buttons to select the target image on the local path. The system automatically calculates the binarization threshold based on the Otsu algorithm and displays the binarized image. At this time, the user can also manually adjust the binarization threshold to obtain the best image by refreshing the binarized image in real time.

Step 3: After the curve recognition is completed, according to the image scale conversion method that was proposed above, input the actual “mountain width” and “mountain height,” respectively, and click the “Comparison” button to obtain the current two-stage calculation result. When all curves are calculated, click the “Summary” button to obtain an overall display of all the crack curves. At this time, the azimuth and displacement values are displayed in the result display area.

Table 1 Monitoring results of the gravel model

Stage	1 → 2	2 → 3	3 → 4	4 → 5
Azimuth	Left 36.62°	Right 63.93°	Left 6.08°	Left 25.63°
Motion displacement	Max = 0.0708 m Min = 0 m	Max = 0.145 m Min = 0.0202 m	Max = 0.1571 m Min = 0 m	Max = 0.2681 m Min = 0 m

Case study

Curve identification test of TECL

In this section, we perform a functional test on the trailing edge crack curve of a landslide to test whether the system can successfully acquire the crack profile curve. We chose a landslide picture, as shown in Fig. 13.

In accordance with the system operating procedures (mentioned in the "Test platform based on QT" section), we have processed Fig. 13. First, we performed the image preprocessing on the landslide picture (Fig. 12), including *image graying* (IG), *image histogram equalization* (IHE), *image median filtering* (IMF), and *image binarization* (IB). The results are shown in Fig. 14.

In the IMF processing, we used 3 × 3 and 9 × 9 structural elements to process the image. From the results (Fig. 14I-c and I-d), it is easy to see that the outline of image I-c is significantly clearer than that of image I-d. Therefore, we use I-c as the image for subsequent processing. In the IB processing, we performed a multi-threshold test that used four thresholds (100, 124, 127, and 160) to process image I-d to obtain four processed images as shown in Fig. 14(I-e, I-f, I-g, and I-h, respectively).

Second, in order to conveniently compare the effects of the IB processing, we performed the second-stage image processing on the above four images (I-e, I-f, I-g, and I-h), including dilation, erosion, Canny edge detection (*Canny ED*), feature recognition (*FR*), and target curve shaping (*TCS*). The feature parameter is set to 2/3. The results are shown in Fig. 15.

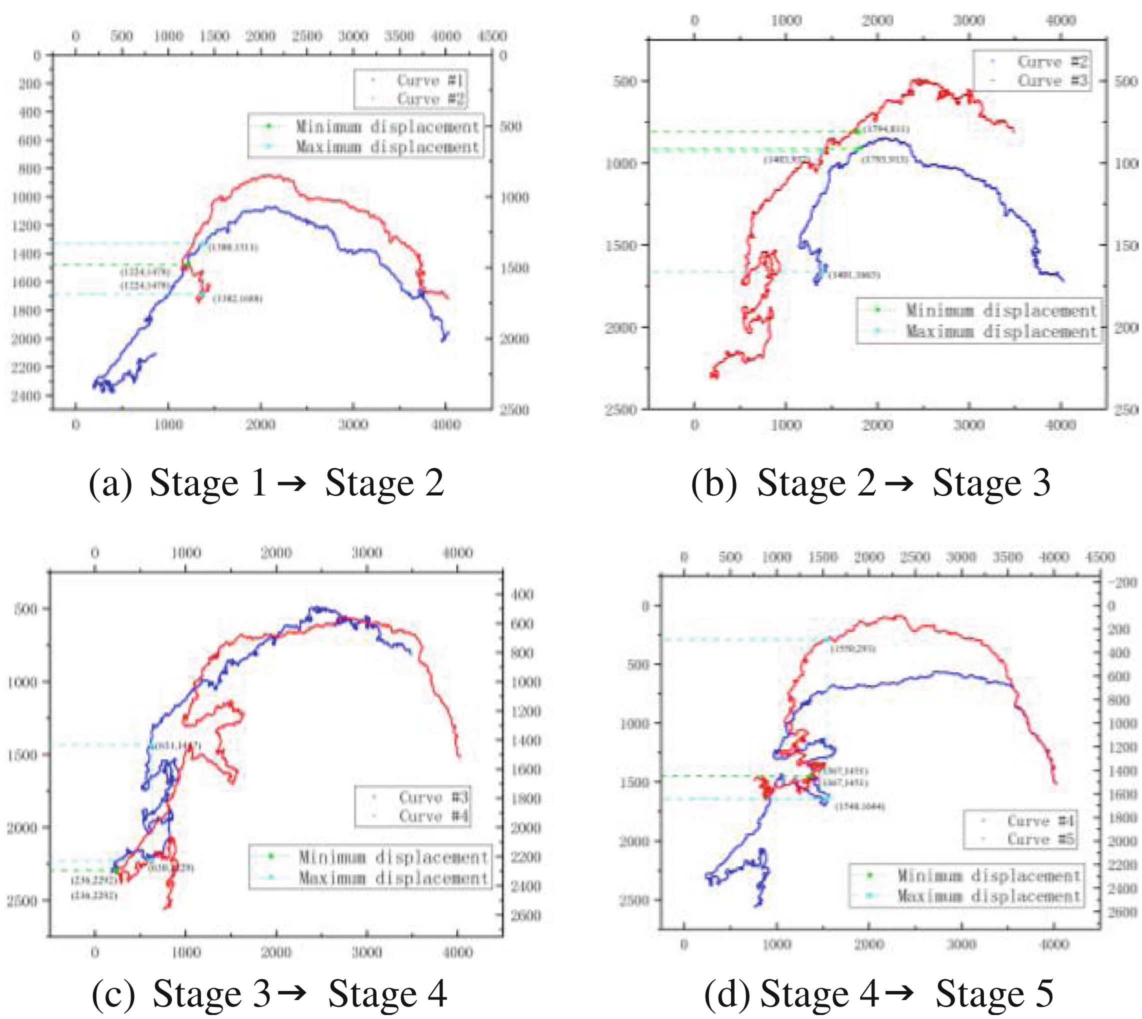

Fig. 20 Curve based on calculated data (gravel model)

Fig. 21 The soil landslide model

As seen from Fig. 15, the proposed method completes the identification of the outline of the TECL. Moreover, from the recognition results, it is seen that different binarization thresholds have different results. For example, we use Otsu's threshold of 124 to generate image II-f5 in which the left portion of the curve is missing (approximately 1/4 of the entire image). The manually set threshold of 100 corresponds to image II-e5, where the curve is completely missing. The manually set threshold of 160 corresponds to image II-h5, where interference information appears at the bottom. The manually set threshold of 127 corresponds to image II-g5, which better outlines the target curve. Therefore, the suggested approach for threshold setting is to first automatically calculate threshold with a computer program and then to manually fine-tune it.

Test of the TECL monitoring

In this section, we designed three models, namely, the computer 3D model, the gravel model, and the soil model, to simulate the movement of the landslide and to test whether the proposed method can monitor the crack. Then, we selected a set of landslide disaster scene images and processed them using this method to test its actual performance.

Computer 3D model

We designed a 3D landslide model (40 m high) with the computer software XStream Vue. According to the steps that were described in the "Curve identification test of TECL" section, the two pictures before and after the landslide are processed (the structural element size is 3 × 3, and the feature parameter is 2/3). The processed images are shown in Fig. 16.

To better show Fig. 16b, we plot the calculated data output from the test platform with the Origin software, as shown in Fig. 17.

From the test results, the slip state of the 3D landslide model can be monitored by the method proposed that is in this paper. We can input the image of the landslide hazard at different stages to obtain the azimuth and displacement values of the crack motion.

Gravel model

The gravel model consists of two parts: fine sand and box. Fine sand is a common building material. The box material is an acrylic sheet, which is a rectangular box with a length of 60 cm, a width of 30 cm, and a height of 60 cm (as shown in Fig. 18). This box simulates a mountain width of 0.6 m.

The gravel is piled into a hill-like shape, and a camera is set 0.5 m in front of the sliding body. The whole model is shaken at a constant time interval to slide it to simulate the movement of a landslide. The motion image of the landslide model is immediately taken. We have selected a total of 5 pictures to form 4 stages of the exercise. We used the method that is proposed in this paper to process the five images. The feature parameters that are used in pictures 1–3, 4, and 5 are 2/3, 1/3, and 1/2, respectively. The results of each stage are shown in Fig. 19 and Table 1.

It should be noted that in this experiment, the camera is close to the model (0.5 m), and the images that we collected have strong graininess, which causes the images to contain too much "white point" noise. Therefore, in IMF processing, we have increased the structural element value (17 × 17).

To better show Fig. 19b, we plot the calculated data output from the test platform with the Origin software, as shown in Fig. 20.

From the test results, it can be seen that the slip state of the gravel landslide model can be monitored by the method that is proposed in this paper. We can input the images of the landslide hazard at different stages (e.g., 4 stages) to obtain the azimuth and displacement values of the crack motion.

Soil landslide model

We used a loose mound on our campus to simulate a soil landslide. This mound has a length of 80 cm, a width of 30 cm, and a height of 50 cm (as shown in Fig. 21). This mound simulates a mountain with a width of 0.8 m. We sprayed black paint on the soil to mark the sliding area. We used a small shovel to move the soil at the bottom of the landslide to simulate the sliding process.

We have selected a total of 5 pictures to form the 4 stages of the exercise. We used the method that is proposed in this paper to process the five images. The feature parameter that is used in pictures 1 and 5 is 1/2, that in pictures 2 and 3 is 2/5, and that in picture 4 is 1/3. The results of each stage are shown in Fig. 22 and Table 2.

To better show Fig. 22b, we plot the calculated data output from the test platform with the Origin software, as shown in Fig. 23.

From the test results, the slip state of the soil landslide model can be monitored by the method that is proposed in this paper. We can input the images of the landslide hazard at different stages (i.e., 4 stages) to obtain the azimuth and displacement values of the crack motion.

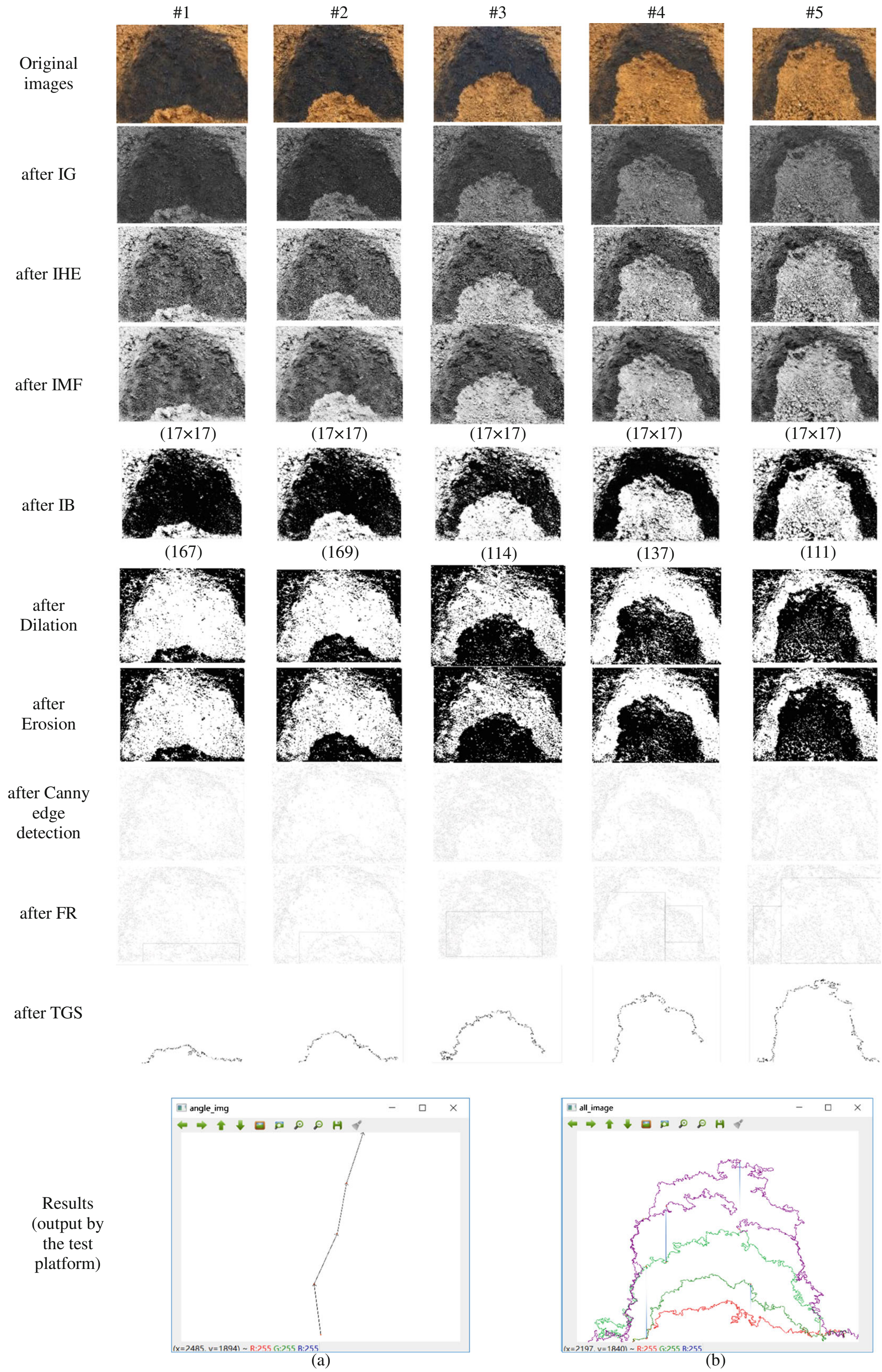

Fig. 22 Processed images of the soil model

Table 2 Monitoring results of the soil model

Stage	1 → 2	2 → 3	3 → 4	4 → 5
Azimuth	Left 7.58°	Right 32.21°	Left 14.14°	Left 7.86°
Motion displacement	Max = 0.1484 m Min = 0 m	Max = 0.272 m Min = 0.0202 m	Max = 0.2114 m Min = 0 m	Max = 0.2545 m Min = 0 m

Panzhihua Airport landslide

On October 3, 2009, a huge landslide took place in the filling body (parts B and C in Fig. 24) of the Panzhihua Airport, China, and led to the reactivation of the Yijiapin ancient landslide (Wang et al. 2013). The landslide was approximately 1600 m long, 200 to 400 m wide, and 10 to 25 m thick, with a total volume of approximately 5.1 million m^3. The landslide moved mainly towards 115° at a slope angle of approximately 20°.

The sliding surface was very loose, with a series of cracks occurring in both the vertical and horizontal directions. Obvious tension fractures and collapses were found at the trailing edge of the sliding body (Fig. 25a).

Starting in November, we conducted a monitoring study of the landslide, where a moving image of a group of collapsed bodies (No. 091206, a landslide that occurred on December 6, 2009) was captured, as shown in Fig. 25b (40 m width). In order to test the effect of the method that is proposed in this paper, we processed the images according to the processing flow in the "Test of the TECL monitoring" section (the structural element size is 9 × 9, and the feature parameter is 2/3). The processed images are shown in Fig. 26.

To better show Fig. 26b, we plot the calculated data output from the test platform with the Origin software, as shown in Fig. 27.

From the test results, the slip state of the real landslide can be monitored by the method that is proposed in this paper. It should be noted that because the image's source shooting angle is inconsistent with that set in this paper, a series of flips are performed on the image source, as shown in Fig. 27.

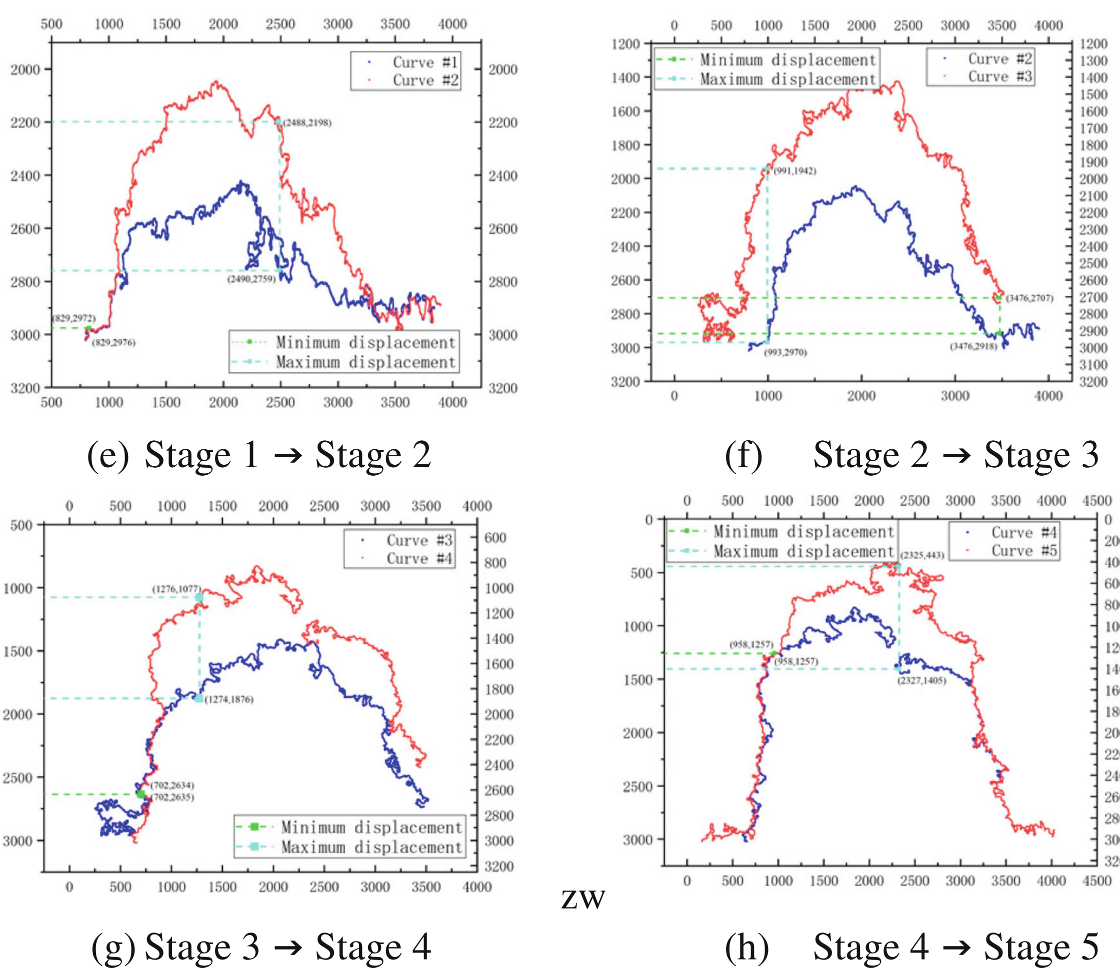

Fig. 23 Curve based on the calculated data (soil model)

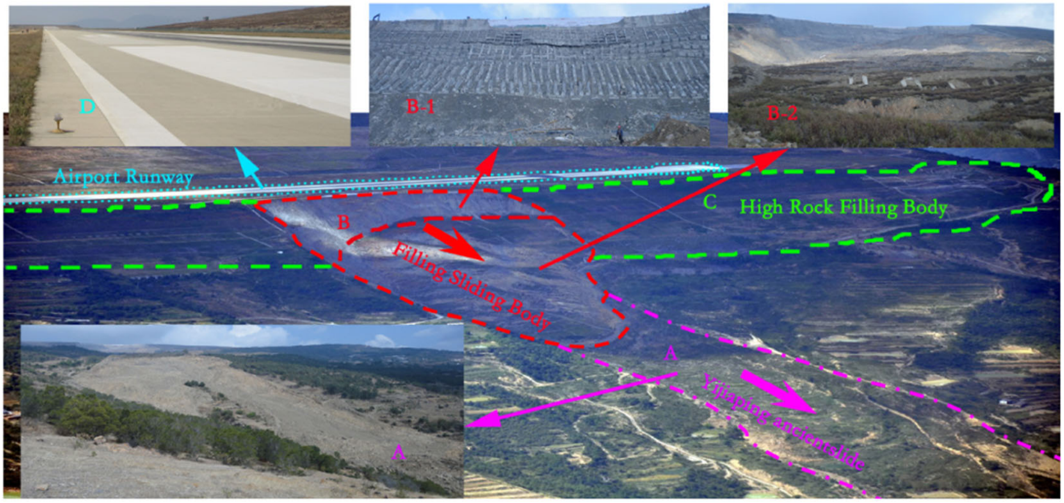

Fig. 24 Aerial photo of the October 3 landslide and its composition in Panzhihua Airport, China (Wang et al. 2013)

Then, we had installed five displacement sensors to monitor the surface cracks at the trailing edge of the landslide (Fig. 28.). Sensor 5 captured the crack curve, as shown in Fig. 29.

The displacement recorded by node No.5 was increasing at a speed of 2.7 mm/h, resulting in a displacement of 231 mm within 86 h (from A1 to A2), which meant that in that location a crack was rapidly opening. At 14:20 on December 7, 2009, an obvious crack and subsidence appeared in the place where the No. 5 monitor was located.

It can be seen from the above comparison that the monitoring results of the two methods are consistent.

Conclusions

Through methods and case studies, we have concluded the following points:

1. The curve recognition method that is proposed in this paper can identify the crack outline of the TEL. The methods include image graying, histogram equalization, median filtering, image binarization (Otsu algorithm), dilation, erosion, and Canny Edge detection. Case III-A demonstrates that this method is feasible.
2. The crack motion expression method that is proposed in this paper can semiquantitatively describe the motion and state of landslide cracks. Specifically, this method includes changes in the azimuth and motion displacement that describe the crack motion. The "interval median comparison" algorithm is also proposed to calculate the azimuth and displacement of the trailing edge curve of the same landslide body in different time periods. Case III-B demonstrates that this method is feasible.
3. The QT platform-based test software that is developed in this paper can monitor the cracks at the trailing edge of the landslide. The user (geologist) only needs to collect images during the landslide's movement to output crack monitoring data through the software's calculations. Compared with the traditional displacement sensor monitoring method, the technology can greatly cover the monitoring blind areas. Compared with the satellite remote sensing methods, the costs are lower, and the operator's professional skill requirements are lower. Overall, the method is simple to install and easy to operate, and the

(a) (b)

Fig. 25 **a** Field photo showing a 15-cm-wide crack at the trailing edge of the landslide. **b** Scene photo of one collapsed body

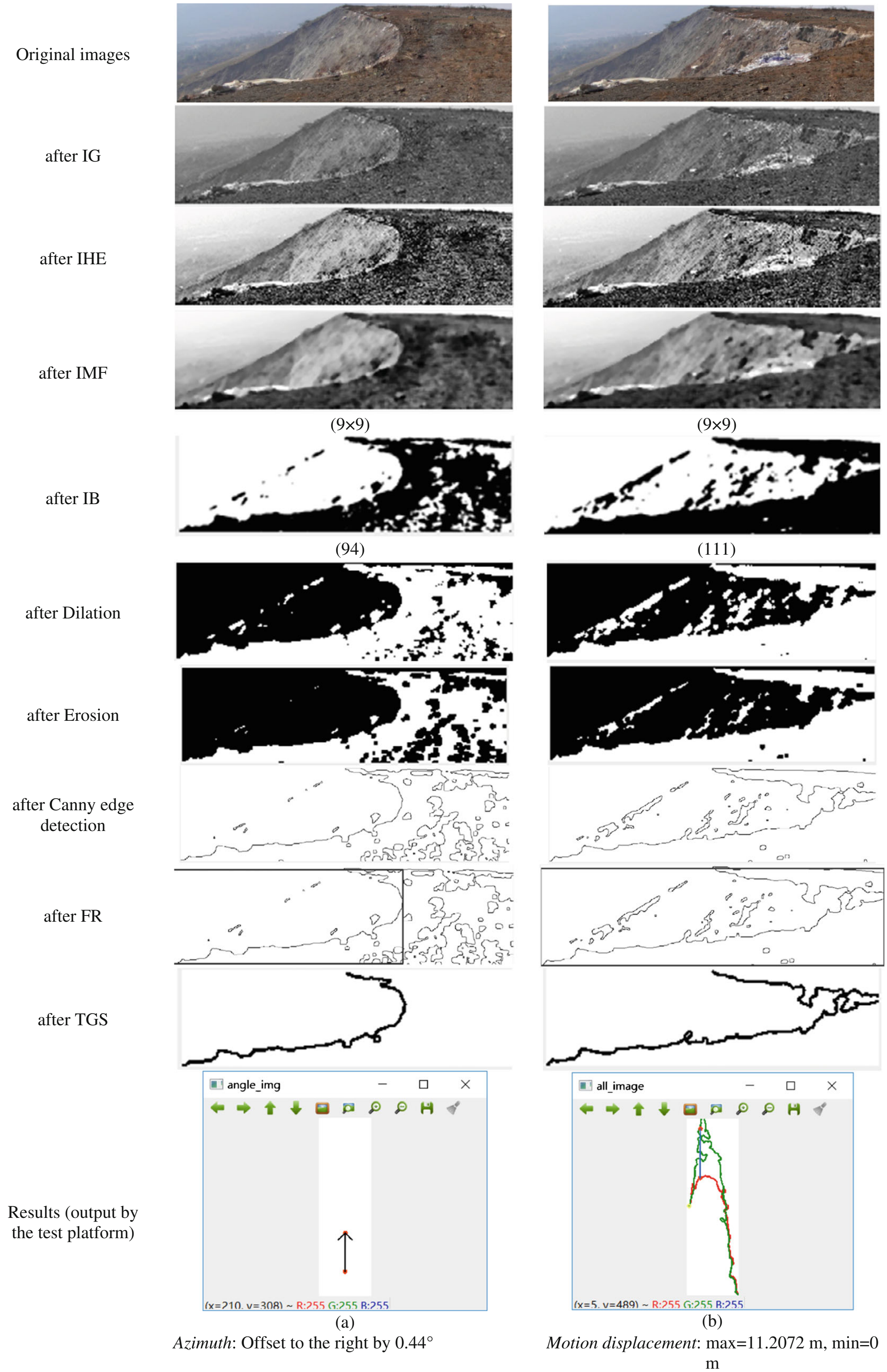

Fig. 26 Processed images of the landslide

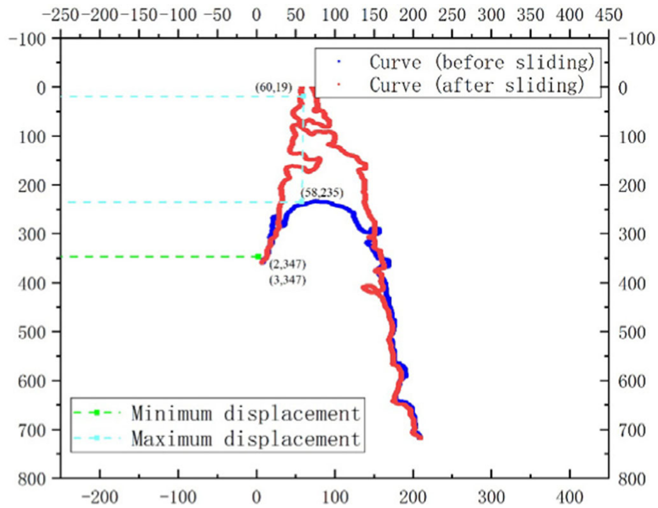

Fig. 27 Curve based on the calculated data (Panzhihua Airport landslide)

method is particularly suitable for on-site monitoring during landslide emergency rescue.

4. There are some limitations in this method when we use it to monitor landslides. One limitation is that the viewing angle may cause a distortion. Since we use multi-temporal images, it is difficult to ensure that the viewing angle of each photo is absolutely consistent, which will lead to displacement monitoring distortions. In addition, for large landslides or landslides with large lateral dimensions, the trailing edge may exceed the camera's viewing angle. The second limitation is that the landslide type may limit the monitoring accuracy, such as loess landslide. We have used the method that is proposed in this paper to carry out image recognition experiments on a loess landslide in Gansu Province. The results show that the color of the stable body of the trailing edge is almost the same as that of the sliding body, which presents a great difficulty for our identification. The third limitation is image registration. Strictly speaking, multi-temporal images require registration to improve accuracy (Feng et al. 2019a). The method proposed in this paper constrains the consistency of image sensors, photographing positions, and viewing angles as much as possible, which may be suitable for on-site emergency landslide monitoring (Travelletti et al. 2012). However, if we conduct long-term deformation observations, we need to study the registration method further (Bentoutou et al. 2005; Feng et al. 2019b).>

It should be pointed out that there is no publicly recognized definition of the azimuth and motion displacement of the landslide body. The curve identification and "interval median comparison" algorithm proposed in this paper to calculate the change in

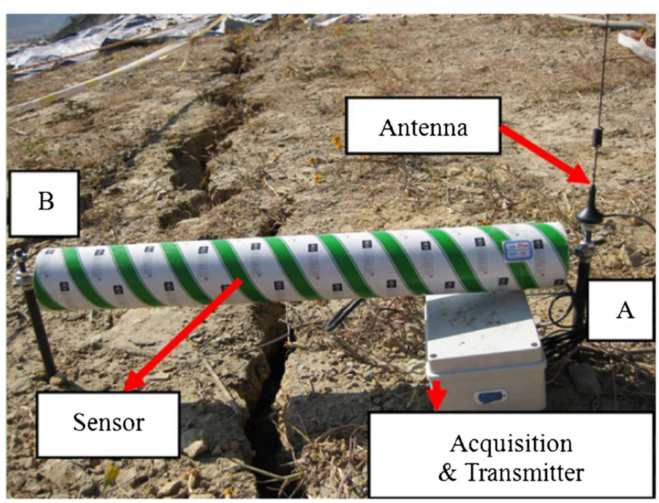

Fig. 28 Photo of the monitor installed (Wang et al. 2013)

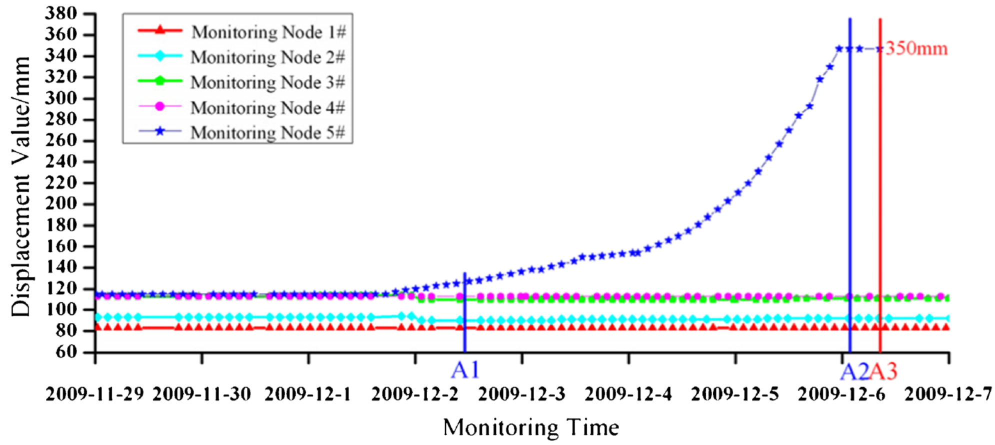

Fig. 29 The displacement value vs. monitoring time (Wang et al. 2013)

the crack displacement at the trailing edge of landslide needs to be further tested and improved.

Acknowledgments

The authors would like to thank graduate students Xiang Wang, Lingyu Meng, Pan Zhong, and Tianxiang Zhuo for their help during the experiment part of the case study. The authors thank the editor Gianvito Scaringi and anonymous reviewers for their helpful comments and suggestions.

Funding informationThis work was sponsored by the National Natural Science Foundation of China under Grant 41521002 and Grant 41704130 and the funds of the Science Plans of Sichuan Province, China, under Grant 2018SZ0347 and Grant 17CZ0004. This research was also partially supported by the China Scholarship Council under Grant 201808510005.

References

Barbarella M, Fiani M (2013) Monitoring of large landslides by terrestrial laser scanning techniques: field data collection and processing. Eur J Remote Sens 46:126–151. https://doi.org/10.5721/EuJRS20134608

Benoit L, Briole P, Martin O et al (2015) Monitoring landslide displacements with the Geocube wireless network of low-cost GPS. Eng Geol 195:111–121. https://doi.org/10.1016/j.enggeo.2015.05.020

Bentoutou Y, Taleb N, Kpalma K, Ronsin J (2005) An automatic image registration for applications in remote sensing. IEEE Trans Geosci Remote Sens 43:2127–2137. https://doi.org/10.1109/TGRS.2005.853187

Briese C (2010) Extraction of digital terrain models. Airborne and Terrestrial Laser Scanning. Whittles Publishing United Kingdom, In, pp 147–150

Canny J (1986) A computational approach to edge detection. IEEE Trans Pattern Anal Mach Intell 8:679–698. https://doi.org/10.1109/ASICON.2011.6157287

Casson B, Delacourt C, Allemand P (2005) Contribution of multi-temporal remote sensing images to characterize landslide slip surface – application to the La Clapière landslide (France). Nat Hazards Earth Syst Sci 5:425–437. https://doi.org/10.5194/nhess-5-425-2005

Centre for Research on the Epidemiology of Disasters - CRED (2019) Natural disasters 2018. CRED, Brussels

Chen H, Zeng Z, Tang H (2015) Landslide deformation prediction based on recurrent neural network. Neural Process Lett 41:169–178. https://doi.org/10.1007/s11063-013-9318-5

Cheng HD, Jiang XH, Sun Y, Wang J (2001) Color image segmentation: advances and prospects. Pattern Recogn 34:2259–2281. https://doi.org/10.1016/S0031-3203(00)00149-7

Cho H-W, Yoon H-J, Yoon J-C (2016) Analysis of crack image recognition characteristics in concrete structures depending on the illumination and image acquisition distance through outdoor experiments. Sensors (Basel) 16. https://doi.org/10.3390/s16101646

Colesanti C, Wasowski J (2006) Investigating landslides with space-borne synthetic aperture radar (SAR) interferometry. Eng Geol 88:173–199. https://doi.org/10.1016/j.enggeo.2006.09.013

De Dios RJC, Enriquez J, Mendoza FGVEA et al (2009) Design, development, and evaluation of a tilt and soil moisture sensor network for slope monitoring applications. In: IEEE region 10 annual international conference. Proceedings/TENCON, IEEE, pp 1–6

Delacourt C, Allemand P, Berthier E et al (2007) Remote-sensing techniques for analysing landslide kinematics: a review. Bull la Soc Geol Fr 178:89–100

Fan X, Xu Q, Scaringi G et al (2017) Failure mechanism and kinematics of the deadly June 24th 2017 Xinmo landslide, Maoxian, Sichuan, China. Landslides 14:2129–2146. https://doi.org/10.1007/s10346-017-0907-7

Feng R, Du Q, Li X, Shen H (2019a) Robust registration for remote sensing images by combining and localizing feature- and area-based methods. ISPRS J Photogramm Remote Sens 151:15–26. https://doi.org/10.1016/j.isprsjprs.2019.03.002

Feng R, Li X, Shen H (2019b) Mountainous remote sensing images registration based on improved optical flow estimation. ISPRS Ann Photogramm Remote Sens Spat Inf Sci 4:479–484. https://doi.org/10.5194/isprs-annals-IV-2-W5-479-2019

Ferrigno F, Gigli G, Fanti R et al (2017) GB-InSAR monitoring and observational method for landslide emergency management: the Montaguto earthflow (AV, Italy). Nat Hazards Earth Syst Sci 17:845–860. https://doi.org/10.5194/nhess-17-845-2017

Frodella W, Ciampalini A, Bardi F, Salvatici T, Traglia F, Basile G, Casagli N (2018) A method for assessing and managing landslide residual hazard in urban areas. Landslides 15:183–197. https://doi.org/10.1007/s10346-017-0875-y

Gance J, Malet JP, Dewez T, Travelletti J (2014) Target detection and tracking of moving objects for characterizing landslide displacements from time-lapse terrestrial optical images. Eng Geol 172:26–40. https://doi.org/10.1016/j.enggeo.2014.01.003

Gatos B, Pratikakis I, Perantonis SJ (2006) Adaptive degraded document image binarization. Pattern Recogn 39:317–327. https://doi.org/10.1016/j.patcog.2005.09.010

Gavilán M, Balcones D, Marcos O et al (2011) Adaptive road crack detection system by pavement classification. Sensors 11:9628–9657. https://doi.org/10.3390/s111009628

Ghuffar S, Székely B, Roncat A, Pfeifer N (2013) Landslide displacement monitoring using 3D range flow on airborne and terrestrial LiDAR data. Remote Sens 5:2720–2745. https://doi.org/10.3390/rs5062720

Guthrie RH, Friele P, Allstadt K et al (2012) The 6 August 2010 Mount Meager rock slide-debris flow, Coast Mountains, British Columbia: characteristics, dynamics, and implications for hazard and risk assessment. Nat Hazards Earth Syst Sci 12:1277–1294. https://doi.org/10.5194/nhess-12-1277-2012

Huang R, Fan X (2013) The landslide story. Nat Geosci 6:325–326. https://doi.org/10.1038/ngeo1806

Iverson RM, George DL, Allstadt K et al (2015) Landslide mobility and hazards: implications of the 2014 Oso disaster. Earth Planet Sci Lett 412:197–208. https://doi.org/10.1016/j.epsl.2014.12.020

James MR, Robson S, d'Oleire-Oltmanns S, Niethammer U (2017) Optimising UAV topographic surveys processed with structure-from-motion: ground control quality, quantity and bundle adjustment. Geomorphology 280:51–66. https://doi.org/10.1016/j.geomorph.2016.11.021

Jiang R, Jáuregui DV, White KR (2008) Close-range photogrammetry applications in bridge measurement: literature review. Meas J Int Meas Confed 41:823–834

Li N (2006) Research on slope monitoring and forecasting based on digital photography and image analysis, Chinese edn. Zhengzhou University

Marr D, Hildreth E (1980) Theory of edge detection. Proc R Soc London Ser B, Contain Pap a Biol character R Soc (Great Britain) 207:187–217. https://doi.org/10.1098/rspb.1980.0020

Massonnet D, Rossi M, Carmona C et al (1993) The displacement field of the Landers earthquake mapped by radar interferometry. Nature 364:138–142. https://doi.org/10.1038/364138a0

Mohammad I, Huang H (2010) Monitoring fatigue crack growth and opening using antenna sensors. Smart Mater Struct 19. https://doi.org/10.1088/0964-1726/19/5/055023

Noferini L, Pieraccini M, Luzi G, et al (2006) Ground-based radar interferometry for monitoring unstable slopes. Int Geosci Remote Sens Symp 4088–4091. https://doi.org/10.1109/IGARSS.2006.1048

Otsu N (1979) A threshold selection method from gray-level histograms. IEEE Trans Syst Man Cybern 9:62–66. https://doi.org/10.1109/TSMC.1979.4310076

Peng B, Jiang Y, Pu Y (2015) Review on automatic pavement crack image recognition algorithms. J Highw Transp Res Dev (English Ed 9:13–20

Pfeiffer J, Zieher T, Rutzinger M et al (2019) Comparison and time series analysis of landslide displacement mapped by airborne, terrestrial and unmanned aerial vehicle based platforms. ISPRS Ann Photogramm Remote Sens Spat Inf Sci 4:421–428. https://doi.org/10.5194/isprs-annals-IV-2-W5-421-2019

Pieraccini M, Luzi G, Atzeni C (2001) Terrain mapping by ground-based interferometric radar. IEEE Trans Geosci Remote Sens 39:2176–2181. https://doi.org/10.1109/36.957280

Pieraccini M, Miccinesi L (2019) Ground-based radar interferometry: a bibliographic review. Remote Sens. 11

Prokop A, Panholzer H (2009) Assessing the capability of terrestrial laser scanning for monitoring slow moving landslides. Nat Hazards Earth Syst Sci 9:1921–1928. https://doi.org/10.5194/nhess-9-1921-2009

Qu Z, Ju F-RR, Guo Y et al (2018) Concrete surface crack detection with the improved pre-extraction and the second percolation processing methods. PLoS One 13:e0201109. https://doi.org/10.1371/journal.pone.0201109

Ramesh MV (2014) Design, development, and deployment of a wireless sensor network for detection of landslides. Ad Hoc Netw 13:2–18. https://doi.org/10.1016/j.adhoc.2012.09.002

Rawat N, Sharma D, Pant D (2017) Geospatial landslide hazard zonation for district Pauri Garhwal, Uttarakhand, India, using quantitative methods. Int J Heal Syst Disaster Manag 5:57–62. https://doi.org/10.4103/ijhsdm.ijhsdm

Riedel PS, Gomes AR, Ferreira MV et al (2010) Identification of landslide scars in the region of the Serra do Mar, São Paulo State, Brazil, using digital image processing and spatial analysis tools. GIScience Remote Sens 47:498–513. https://doi.org/10.2747/1548-1603.47.4.498

Rothmund S, Vouillamoz N, Joswig M (2017) Mapping slow-moving alpine landslides by UAV — opportunities and limitations. Lead Edge 36:571–579. https://doi.org/10.1190/tle36070571.1

Saravanan C (2010) Color image to grayscale image conversion. 2010 2nd Int Conf Comput Eng Appl ICCEA 2010 2:196–199. https://doi.org/10.1109/ICCEA.2010.192

Sezgin M, Sankur B (2004) Survey over image thresholding techniques and quantitative performance evaluation. J Electron Imaging 13:146–166. https://doi.org/10.1117/1.1631316

Sim KS, Tso CP, Tan YY (2007) Recursive sub-image histogram equalization applied to gray scale images. Pattern Recogn Lett 28:1209–1221. https://doi.org/10.1016/j.patrec.2007.02.003

Stumpf A, Malet JP, Allemand P et al (2015) Ground-based multi-view photogrammetry for the monitoring of landslide deformation and erosion. Geomorphology 231:130–145. https://doi.org/10.1016/j.geomorph.2014.10.039

Stumpf A, Malet JP, Kerle N et al (2013) Image-based mapping of surface fissures for the investigation of landslide dynamics. Geomorphology 186:12–27. https://doi.org/10.1016/j.geomorph.2012.12.010

Sun T, Neuvo Y (1994) Detail-preserving median based filters in image processing. Pattern Recogn Lett 15:341–347. https://doi.org/10.1016/0167-8655(94)90082-5

Tao C, Kaikuang M, Lihui C (1999) Tri-state median filter for image denosing. IEEE Trans Image Process 8:1834–1838

Tarchi D, Casagli N, Fanti R et al (2003) Landslide monitoring by using ground-based SAR interferometry: an example of application to the Tessina landslide in Italy. Eng Geol 68:15–30. https://doi.org/10.1016/S0013-7952(02)00196-5

Travelletti J, Delacourt C, Allemand P et al (2012) Correlation of multi-temporal ground-based optical images for landslide monitoring: application, potential and limitations. ISPRS J Photogramm Remote Sens 70:39–55. https://doi.org/10.1016/j.isprsjprs.2012.03.007

Wadge G (2003) A strategy for the observation of volcanism on Earth from space. Philos Trans R Soc A Math Phys Eng Sci 361:145–156. https://doi.org/10.1098/rsta.2002.1117

Wang B, Zhao W, Gao P et al (2018) Crack damage detection method via multiple visual features and efficient multi-task learning model. Sensors (Switzerland) 18:1–18. https://doi.org/10.3390/s18061796

Wang C (2009) Disaster phenomena of Wenchuan earthquake in high resolution airborne synthetic aperture radar images. J Appl Remote Sens 3:031690. https://doi.org/10.1117/1.3154558

Wang H, Tuo X, Zhang G, Peng F (2013) Panzhihua airport landslide (Oct. 3rd 2009) and an emergency monitoring and warning system based on the internet of things. J Mt Sci 10:873–884. https://doi.org/10.1007/s11629-013-2368-3

Xu Q, Dong X, Li W (2019) Integrated space-air-ground early detection, monitoring and warning system for potential catastrophic geohazards. Geomatics Inf Sci Wuhan Univ 44:957–966

Yang X, Chen L (2010) Using multi-temporal remote sensor imagery to detect earthquake-triggered landslides. Int J Appl Earth Obs Geoinf 12:487–495. https://doi.org/10.1016/j.jag.2010.05.006

Yin Y, Wang F, Sun P (2009) Landslide hazards triggered by the 2008 Wenchuan earthquake, Sichuan, China. Landslides 6:139–152. https://doi.org/10.1007/s10346-009-0148-5

Yin Y, Wang H, Gao Y, Li X (2010) Real-time monitoring and early warning of landslides at relocated Wushan Town, the Three Gorges Reservoir, China. Landslides 7:339–349. https://doi.org/10.1007/s10346-010-0220-1

Zhou P (2004) Indicator system and techniques of landslide monitoring. J Geom 10:19–26

H. Wang (✉)
State Key Laboratory of Geohazard Prevention and Geoenvironment Protection,
Chengdu University of Technology,
Chengdu, 610059, People's Republic of China
Email: wanghh@cdut.edu.cn

H. Wang · Y. Zhong
Department of Civil and Environmental Engineering,
University of California at Berkeley,
Berkeley, CA 94720, USA

Y. Zhong
e-mail: zys@berkeley.edu

D. Nie
School of Nuclear Technology and Automation Engineering,
Chengdu University of Technology,
Chengdu, 610059, People's Republic of China
e-mail: 740398568@qq.com

X. Tuo
Chengdu University of Technology,
Chengdu, People's Republic of China
e-mail: tuoxianguo@suse.edu.cn

X. Tuo
School of Automation and Information,
Sichuan University of Science and Engineering,
Zigong, 643000, People's Republic of China